Title

^{17}O NMR as a Tool in Discrete Metal Oxide Cluster Chemistry

Authors

Ohlin, CA

Casey, WH

Publication Date

2018

DOI

10.1016/bs.arnmr.2018.01.001

Peer reviewed

CHAPTER FIVE

^{17}O NMR as a Tool in Discrete Metal Oxide Cluster Chemistry

C. André Ohlin*, William H. Casey†
*Umeå University, Umeå, Sweden
†University of California, Davis, CA, United States

Contents

Abstract

This chapter covers recent developments in ^{17}O NMR spectroscopy as applied to discrete metal oxide clusters, particularly in the context of their use as models in geochemistry and catalysis. Dynamic ^{17}O NMR methods based on the McConnell–Bloch equations are explored in depth, and recent advances are reviewed. High-pressure NMR methods are also discussed and reviewed, as are recent developments in the use of density functional theory in the computation of ^{17}O NMR shifts in polyoxometalates. The emphasis of the chapter is on the new developments that promise to reinvigorate ^{17}O NMR as a central tool in the study of aqueous chemical kinetics, with the most urgent challenges being understanding the rates of isotopic substitution into bridging oxygens in clusters.

Keywords: ^{17}O NMR, Polyoxometalates, Solution dynamics, Kinetics, Water, Minerals, Metal oxides, Geochemistry, High-pressure NMR

Annual Reports on NMR Spectroscopy, Volume 94
ISSN 0066-4103
https://doi.org/10.1016/bs.arnmr.2018.01.001

1. INTRODUCTION

On the face of it, ^{17}O NMR spectrometry as a technique suffers from a lot of disadvantages: the natural abundance is very low (<0.04%), it is a quadrupolar nucleus and the generally fast transverse relaxation times yield broad signals. However, modern high-field NMR spectrometers are sufficiently sensitive that spectra can be sometimes be collected on oxygen-containing molecules without the need for artificial isotopic enrichment—although molar concentrations may need to be high—and while the line width of, for example, the oxygen signal in water is close to 70 Hz, the shift range is very large—spanning well over 1000 ppm for even simple metal oxides. While the very short T_1, typically tens of milliseconds, can make multipulse experiments difficult, it does allows for the quick collection of a large number of repeated scans in single-pulse experiments, which partly offsets the low natural abundance of ^{17}O.

As a consequence, ^{17}O NMR spectrometry is a tool which is sensitive towards the environment of the oxygen site and can be used to investigate the chemistry of different types of organic and inorganic oxides in solution. Due to the cost of enriched reagents, it is primarily inorganic oxides which are accessible as enriched products, and due to this and the central role of structural oxygen atoms in this class of materials, ^{17}O NMR is particularly important in inorganic chemistry.

Here we will provide a general overview of recent advances in experimentation involving ^{17}O NMR spectrometry, and we will provide a very specific focus on the use of NMR spectrometry in investigating the chemistry of discrete metal oxide clusters in solution, and on new efforts to extend the results to gigapascal (GPa) pressures. This latter subject is highly important in light of the historical use of activation volumes determined via ^{17}O NMR experiments to assign mechanisms of inorganic ligand exchange reactions, and new work to unravel protein structures via high-pressure denaturing. The relevance of high pressure to geochemistry is also key to these new efforts as the developments open up a whole new unexplored region of aqueous solution chemistry to science.

The combination of the central role that oxygen plays in the chemistry of discrete metal oxide clusters with the difficulty of performing multidimensional experiments to assign NMR signals to specific sites gives computational shift assignment an important role. The sizes of the clusters in question make density functional theory (DFT) the only viable

computational method to assign some chemical shifts. We will present recent advances in the computation of ^{17}O NMR chemical shifts in discrete metal oxide clusters by DFT with a focus on practical approaches to doing so.

2. ^{17}O AS A NUCLEUS IN METAL OXIDE CLUSTER CHEMISTRY

^{17}O has a natural abundance of ca 0.04%, is the only NMR active nucleus of oxygen and has a spin of $I = 5/2$, gyromagnetic ratio of -3.6×10^{-7} s^{-1} T^{-1} and a quadrupole moment of -2.6 fm^2 [1]. The presence of a quadrupole moment leads to signals that are comparatively broad; however, the large shift range makes it a powerful tool in studying the chemistry of oxygen-containing compounds. For example, while a typical line width of the oxygen site in $H_2^{17}O$ is ca 70 Hz, corresponding to ca 1.3 ppm on a 9.4-T instrument, a discrete metal oxide cluster such as $[Nb_{10}O_{28}]^{6-}$ has signals covering a shift window of over 700 ppm [2]. In addition, for smaller, symmetrical molecules, signal widths are often quite narrow.

^{17}O has a very short longitudinal or spin-lattice relaxation time, T_1 (ca 20 ms for $H_2^{17}O$), which creates both opportunities and problems. While relaxation is fast and allows for the acquisition of many scans in a short amount of time, this also makes certain experiments where retention of magnetisation is important—such as diffusion experiments—very challenging. Since T_1 is dependent on the rotational correlation of the analyte, T_1 can be increased somewhat by working with low-viscosity solvents and at elevated temperatures, and may lead to sharper line widths.

To overcome the low natural abundance of ^{17}O (0.04%), target molecules can be enriched. While this can be costly, with 20% enriched $H_2^{17}O$ selling for ca USD 600 per gram, it affords access to the detection and characterisation of the environment of one of the most common—and arguably most important—elements in nature.

Polyoxovanadates have long been studied by NMR owing the sensitivity and natural abundance of the ^{51}V nucleus, coupled with a large spectral window. ^{95}Mo, ^{97}Mo and ^{183}W NMR have likewise been useful techniques in resolving solution chemistry for polyoxomolybdates and -tungstates. Polyoxoniobates and -tantalates, however, lack this advantage, since ^{93}Nb and ^{181}Ta are quadrupolar nuclei which yield broad NMR signals that cover a large portion of the spectral window, and exhibit low sensitivity. All of

these oxide clusters do contain oxygen atoms though, making ^{17}O NMR an attractive technique for studying polyoxometalates in solution.

The utility of ^{17}O NMR in studying the solution chemistry of discrete metal oxide clusters, such as polyoxometalates, was recognised early but became practicable only once the transition from continuous wave (CW) to pulsed Fourier-transform (FT) NMR techniques had been made, in conjunction with the availability of ^{17}O-enriched materials [3].

There are a range of uses for ^{17}O NMR in polyoxometalate chemistry, but the chief ones are as a structural probe, as a speciation probe, and as a kinetic probe. These latter two aspects will be covered in Sections 3 and 4, following a brief introduction of classical methods for determination of exchange kinetics by NMR in Sections 2.1–2.3. The use of ^{17}O NMR as a structural probe requires accurate assignment of observed signals, something for which computational methods are becoming increasingly important. This will be covered in Section 5.

2.1 The Classical Vector Model of Nuclear Magnetic Resonance

The NMR experiment can be treated at different levels of theory, ranging from classical physics to quantum mechanics. Depending on the chosen level of theory, different practical approaches can be used, such as the Bloch vector model or product operator formalism. While the former does not apply to coupled spin systems, its conceptual simplicity and applicability to uncoupled spin systems, such as is often effectively the case in ^{17}O NMR experiments, have made it a common approach in kinetic studies of solution dynamics of inorganic coordination compounds and discrete metal oxide clusters. As was made clear in a recent paper [4], even a cell phone now easily has enough power to run the software to simulate spectra via the Bloch–McConnell equations. Much of ^{17}O NMR applied to kinetics relies on this vector model of magnetic relaxation, leading to the Swift–Connick equations of solution chemistry. For this reason, we review the model here as an introduction to ^{17}O NMR and chemical kinetics.

The Bloch vector model is based on the torque equation [5]. In the laboratory frame of reference, for a nucleus with a nonzero magnetic moment, $I \neq 0$, the torque Eq. (1) describes the change in magnetic moment, $\vec{M}$, on application of a magnetic field, $\vec{B}$. Here γ is the gyromagnetic ratio of the nucleus, and $\vec{M} = \begin{bmatrix} M_x \\ M_y \\ M_z \end{bmatrix}$.

$$\frac{d}{dt}\vec{M} = \gamma \cdot \vec{M}(t) \times \vec{B}(t) \tag{1}$$

In the case of a pulsed NMR experiment, the NMR spectrometer magnet provides a permanent, or static, magnetic field, $\vec{B}_0$, along the longitudinal z-axis with a magnitude of $|B_0|$, and an oscillating radio frequency field, $\vec{B}_1$, along the x-axis in the transverse plane, so that $\vec{B} = \vec{B}_0 + \vec{B}_1$. The expanded form of Eq. (1) is shown in Eq. (2), where ω_{rf} is the angular frequency of the applied field.

$$\frac{d}{dt}\vec{M} = \gamma \cdot \begin{bmatrix} M_x \\ M_y \\ M_z \end{bmatrix} \times \begin{bmatrix} |B_1| \cdot \cos(\omega_{rf} \cdot t) \\ -|B_1| \cdot \sin(\omega_{rf} \cdot t) \\ |B_0| \end{bmatrix} \tag{2}$$

The Rabi and Larmor frequencies are then $\omega_1 = \gamma \cdot |B_1|$ and $\omega_0 = \gamma \cdot |B_0|$, respectively, and the system can be solved for the rotating frame after the application of a rotation matrix and introduction of the longitudinal T_1 and transverse T_2 relaxation terms. This procedure yields the familiar form of the Bloch equations shown in Eqs 3–5, where u and v are the real (dispersive) and imaginary (absorptive) parts of the magnetisation in the *rotating transverse plane*, and M_z the magnetisation in the *longitudinal axis*, with $M_z^{eq.}$ being the equilibrium magnetisation along longitudinal axis. When the oscillating radio frequency field is applied, i.e., during a pulse, then $\omega_1 > 0$, and in the absence of an applied field $\omega_1 = 0$.

$$\frac{d}{dt}u(t) = -\frac{u(t)}{T_2} - v(t) \cdot (\omega_{rf} - \omega_0) \tag{3}$$

$$\frac{d}{dt}v(t) = -\frac{v(t)}{T_2} + u(t) \cdot (\omega_{rf} - \omega_0) - M_z(t) \cdot \omega_1 \tag{4}$$

$$\frac{d}{dt}M_z(t) = -\frac{M_z(t) - M_z^{eq.}}{T_1} + v(t) \cdot \omega_1 \tag{5}$$

Although the applicability of the classical Bloch equations is somewhat limited compared to modern treatments of the NMR experiment, they can be easily solved and modified to include chemical exchange using McConnell formalism. In particular, standard one-pulse experiments can generally be treated as if they were low-power continuous-wave experiments, in which case all derivatives equal zero so that the Bloch equations cease to be differential equations. Similarly, if there is no applied field

present, then the contribution of M_z becomes decoupled from the magnetisation in the transverse plane and can be ignored when solving the equations.

The two assumptions are, however, mutually exclusive, as in the CW case the applied field is always on and $M_z(t)$ is a constant for which an arbitrary value can normally be chosen. Either assumption presents different strategies for exact solutions depending on the type of experiment being modelled.

The Bloch equations can be further rewritten by defining a term for the transverse magnetisation, $M_{uv} = u + i \cdot v$. This reduces by one the number of differential equations that need to be solved. It also has a natural intuitive feel, as it treats the magnetisation in the transverse plane as one entity that is distinct from the magnetisation in the longitudinal axis. In terms of an NMR experiment, the transfer of magnetisation into the transverse plane is our observable parameter. This situation is in contrast with the longitudinal magnetisation, which typically has to be inferred, rather than measured directly. The magnetisation in the longitudinal axis is not irrelevant though, as it affects the magnitude of the observed signal, as well as being important in multipulse experiments where relaxation along the longitudinal axis is incomplete.

Either way, Eqs (3)–(5) can be rewritten as Eq. (6).

$$\frac{d}{dt}M_{uv}(t) = \left(\omega_{rf} - \omega_0\right) \cdot \left(-v(t) - \frac{u(t)}{T_2} + i \cdot u(t)\right) + i \cdot \left(M_z \cdot \omega_1 - \frac{v(t)}{T_2}\right) \tag{6}$$

Because $u(t) = M_{uv}(t) - i \cdot v(t)$, Eq. (6) further simplifies to Eq. (7), where $\Delta\omega = \omega_{rf} - \omega_0$.

$$\frac{d}{dt}M_{uv} = -\left(\frac{1}{T_2} - i \cdot \Delta\omega\right) \cdot M_{uv} + i \cdot M_z \cdot \omega_1 \tag{7}$$

While this form is particularly useful when discussing low-power CW cases where the time dependence of M_z can be ignored since it is assumed to have a constant magnitude, the different magnetisation terms will be kept separate in the discussion that follows.

Using the derived equations it is trivial to model a simple NMR experiment using, e.g., MATLAB [6] or GNU Octave [7], and analytical

solutions can be obtained using Computer Algebra Systems such as Mathematica [8], Maple [9] or Maxima [10].

2.2 Exchange Kinetics

McConnell showed that chemical exchange under equilibrium conditions can be included in the Bloch equations by modifying the corresponding rate laws [11].

Since for uncoupled systems the total magnetisation is additive—that is $u_{sys.} = \sum_i u_i$, $v_{sys.} = \sum_i v_i$ and $M_{zsys.} = \sum_i M_{zi}$—and the magnetisation in the case of a perfect square pulse covering all frequencies correlates directly with the concentration, all that remains is to recast the time dependence of the magnetisation in the Bloch equations to include the parameters for exchange.

For a system of two species, A and B, in equilibrium, $A \rightleftharpoons B$, the corresponding rate law equations are as shown in Eqs (8) and (9).

$$\frac{d}{dt}[A](t) = -k_A \cdot [A](t) + k_B \cdot [B](t) \tag{8}$$

$$\frac{d}{dt}[B](t) = k_A \cdot [A](t) - k_B \cdot [B](t) \tag{9}$$

Assuming that the magnetisation factors scale equally with concentration for both species, and that they are in equilibrium, then the magnetisation transfer for A in each axis can be written as in Eqs (10)–(12).

$$0 = -k_A \cdot u_A(t) + k_B \cdot u_B(t) \tag{10}$$

$$0 = -k_A \cdot v_A(t) + k_B \cdot v_B(t) \tag{11}$$

$$0 = -k_A \cdot M_{zA}(t) + k_B \cdot M_{zB}(t) \tag{12}$$

Eqs (3)–(5) can then be written as in Eqs (13)–(15) for A.

$$\frac{d}{dt}u_A(t) = -\frac{u_A(t)}{T_{2A}} - v_A(t) \cdot \left(\omega_{tf} - \omega_{0A}\right) - k_A \cdot u_A(t) + k_B \cdot u_B(t) \tag{13}$$

$$\frac{d}{dt}v_A(t) = -\frac{v_A(t)}{T_2} + u_A(t) \cdot \left(\omega_{tf} - \omega_{0A}\right) - M_{zA}(t) \cdot \omega_1 - k_A \cdot v_A(t) + \mathrm{k}_B \cdot v_B(t) \tag{14}$$

$$\frac{d}{dt}M_{zA}(t) = -\frac{M_{zA}(t) - M_z^{eq} \cdot A}{T_{1A}} + v(t) \cdot \omega_1 - k_A \cdot M_{zA}(t) + k_B \cdot M_{zB}(t) \tag{15}$$

The equations for u_B, v_B and M_{zB} are analogous, with the signs preceding k_A and k_B being swapped.

Using u as an example, because $k_B = \frac{k_A \cdot u_A}{u_B}$, if we define $p_{\underline{A}}{}_{B} = \frac{u_A}{u_B}$, then $k_B = p_{\underline{A}}{}_{B} \cdot k_A$. This holds true for v and M_z as well. Eqs (13)–(15) then are rewritten as Eqs (16)–(18).

$$\frac{d}{dt}u_A(t) = -\frac{u_A(t)}{T_{2A}} - v_A(t)\cdot\left(\omega_{rf} - \omega_{0A}\right) - k_A \cdot \left(u_A(t) - p_{\underline{A}}{}_{B} \cdot u_B(t)\right) \tag{16}$$

$$\frac{d}{dt}v_A(t) = -\frac{v_A(\mathrm{t})}{T_2} + u_A(t)\cdot\left(\omega_{rf} - \omega_{0A}\right) - M_{zA}(t)\cdot\omega_1 - k_A \cdot \left(v_A(t) - p_{\underline{A}}{}_{B} \cdot v_B(t)\right) \tag{17}$$

$$\frac{d}{dt}M_{zA}(t) = -\frac{M_{zA}(t) - M_{zA}^{eq.}}{T_{1A}} + v(t)\cdot\omega_1 - k_A \cdot \left(M_{zA}(t) - p_{\underline{A}}{}_{B} \cdot M_{zB}(t)\right) \tag{18}$$

In addition to Eqs (16)–(18), which describe the evolution of magnetisation for species A, there is an analogous set of equations for species B.

It is important to note that there is a critical assumption that any magnetic environment other than A or B being short-lived enough that it can be ignored and do not alter any of the magnetisation terms. For a pulsed experiment that means that exchange should be slow relative to the life time of the applied pulse [4]. Additional assumptions are that the Law of Detailed Balance applies, and—in the above example—that the reactions are first-order and simple (this latter assumption can be addressed by using the appropriate rate law for more higher-order reactions).

In spite of these assumptions the McConnell–Bloch equations have proven remarkably versatile in resolving the kinetics of chemical exchange, and they can be modified to account for complex systems, although these may require the use of a Computer Algebra System, such as Mathematica [8] or Maxima [10], to obtain an analytical solution.

As with the unmodified Bloch equations, the equations can be rewritten by combining the components of the magnetisation of each species in the transverse plane into a single expression, as in Eq. (19).

$$\frac{d}{dt}M_{wA} = -\left(\frac{1}{T_{2A}} - i\cdot\Delta\omega_A\right)\cdot M_{wA} + i\cdot M_{zA}\cdot\omega_1 - \left(p_{\underline{A}\atop B}k_A M_{wB} - M_{wA}k_A\right) \tag{19}$$

Using the simple approach of the McConnell–Bloch equations a wide range of types of kinetic NMR experiments can be modelled. Of particular interest here are a few key examples.

In case signals for two exchanging sites are found close to one another, varying the temperature may lead to coalescence of the signals into one. In this case, Eq. (19) (or Eqs 16 and 17) will accurately describe the profile of the spectrum as a function of temperature using the CW assumption and can be solved to yield an analytical expression (two, in the case of using Eqs 16 and 17) that can be used to fit the entire spectrum at each temperature. Such an approach, although for a more complex system, was used by Johnson et al. to derive rates of fluxionality for a huge uranyl-peroxo cluster, $Na_{30}[(UO_2)_{24}(O_2)_{24}(HP_2O_7)_6(H_2P_2O_7)_6]\cdot nH_2O$ [12].

For well-separated signals this approach does not work, however. In the case of the uranyl ion, $[U(=O)_2(OH)_4]^{2-}$, the ^{17}O signal from the –yl oxygen atoms is found at ca 1100 ppm, whereas the ^{17}O signal from water is used as the shift reference and is defined as 0 ppm. In studying the exchange between the –yl oxygen and bulk water the coalescence method thus cannot be used. Harley et al. obtained rates of exchange by using a saturation-transfer technique [13]. Here, by use of a selective π pulse the net magnetisation of the bulk water signal was inverted. A variable mixing delay was introduced, during which exchange occurring between the relaxed –yl oxygen and the inverted water signal led to a decrease in net magnetisation of the –yl signal, and a $\pi/2$ observation pulse yielded a spectrum which could be interpreted to yield rates of exchange.

Because the exchange involves transfer of magnetisation in the longitudinal plane, the salient equations focus on M_z, as shown in Eqs (20) and (21). Key are the initial values of M_{ZA} and M_{ZB}, which are $M_{z_A}^{eq.}$ and $-M_{z_B}^{eq.}$, respectively, when A is the –yl nucleus and B is the bulk water signal.

$$\frac{d}{dt}M_{zA}(t) = -\frac{M_{zA}(t) - M_{z_A}^{eq.}}{T_{1A}} - k_A\cdot\left(M_{zA}(t) - p_{\underline{A}\atop B}\cdot M_{zB}(t)\right) \tag{20}$$

$$\frac{d}{dt}M_{zB}(t) = -\frac{M_{zB}(t) - M_{z_B}^{eq.}}{T_{1B}} - k_A\cdot\left(-M_{zA}(t) + p_{\underline{A}\atop B}\cdot M_{zB}(t)\right) \tag{21}$$

Solving these equations yields equations that describe the intensities of the two signals as a function of mixing time for a given rate of exchange.

In the previous example the signals were well separated, and providing a selective pulse that only affects one of the signals is possible. When the signals are closer in shift, but still do not exhibit the separation/coalescence behaviour necessary for the simplest two-site model, other techniques are required. While there are multipulse techniques for selective saturation, working with strongly saline aqueous solutions such as those used with polyoxometalates and similar species presents a particular challenge in that they can heat up during the pulse, in which case the change in temperature leads to the pulses becoming decalibrated, and the experiment failing.

A system that presented this challenge is the $[U(=O)_2(CO_3)_3]^{4-}$ molecule, which undergoes exchange with free carbonate. While the ^{13}C signals of free and bound carbonate were found to be separated by a few ppm, no coalescence was found at elevated temperature. Here, a three-pulse approach was used, which exploited the difference in the rotation of the magnetisation in the transverse plane between signals which are on- and off-resonance.

As can be seen in Eqs (3)–(5), if $(\omega_{rf} - \omega_0) = 0$, then $u(t)$ will remain 0 throughout the experiment. The degree to which $u(t)$ will deviate from zero thus depends on the difference between ω_{rf} and ω_0, which is the separation between the pulse and signal in terms of angular frequencies, a phenomenon which is called nutation. Thus, by making one of the signals, that of free carbonate, the on-resonance signal, then the off-resonance nucleus will nutate at a predictable rate. In the experiment by Harley et al. [14], a $\pi/2$ pulse was applied which was on-resonance with respect to the free carbonate. This was followed by second pulse $\pi/2$ after a delay which allowed the $\nu(t)$ to invert for the bound carbonate, while that of the free carbonate was unaffected. This second $\pi/2$ pulse thus caused all the net magnetisation of the two sites to lie along the longitudinal axis again, but with the net magnetisation of the free carbonate inverted relative to the equilibrium state while the net magnetisation of the bound carbonate was returned to the equilibrium state, a situation similar to that in the preceding example.

Thus, following a mixing delay an observation pulse was applied, and the rate of exchange could be determined by solving Eqs (20) and (21) and fitting the intensities of the carbonate signals to the resulting function.

Next, another scenario will be explored, where rates of exchange for ligands bound to paramagnetic centres can be investigated using a technique which exploits the properties of the paramagnetic centre.

2.3 Solvent Exchange in Paramagnetic Systems

The Swift–Connick model [15] is a special case of the Bloch–McConnell equations in that it attempts to resolve the ligand exchange kinetics in systems with paramagnetic ions. More specifically, it was developed in order to look at aqua ligand exchange on paramagnetic metal hexaaqua ions, such as $[Co(H_2O)_6]^{2+}$, where only the bulk water signal can be observed, and the rate of exchange has to be inferred from the temperature-dependent broadening of this bulk water signal. Because of the keen interest in assigning mechanisms to water exchange reactions for first-row transition metals, the Swift–Connick model really became indispensible to chemists studying the ^{17}O NMR of aqueous solutions.

Although it normally is used in studying the exchange between two species, the Swift–Connick model begins by assuming that there are three species present: bulk water, and bound water in two types of paramagnetic environments. It is also assumed that the experiment occurs under CW conditions, and although this is rarely the case these days, single-pulse experiments can generally be modelled using these assumptions.

Here we will return to Eq. (19) since the time dependence of M_z can be ignored, and since we work under CW conditions all time-dependent derivatives are equal to zero. The expressions for three exchanging species A, B and C become Eqs (22)–(24), where k_{XY} is the rate constant for exchange from X to Y.

$$-\left(\frac{1}{T_{2A}} - i\cdot\Delta\omega_A - (k_{AB}+k_{AC})\right)\cdot M_{uvA} - (k_{BA}M_{uvB} + k_{CA}M_{uvC}) = i\cdot M_{zA}\cdot\omega_1 \tag{22}$$

$$-\left(\frac{1}{T_{2B}} - i\cdot\Delta\omega_B - (k_{BC}+k_{BA})\right)\cdot M_{uvB} - (k_{AB}M_{uvA} + k_{CB}M_{uvC}) = i\cdot M_{zB}\cdot\omega_1 \tag{23}$$

$$-\left(\frac{1}{T_{2C}} - i\cdot\Delta\omega_C - (k_{CA}+k_{CB})\right)\cdot M_{uvC} - (k_{BC}M_{uvB} + k_{AC}M_{uvA}) = i\cdot M_{zC}\cdot\omega_1 \tag{24}$$

By defining $L_A = \left(\frac{1}{T_{2A}} - i\cdot\Delta\omega_A - (k_{AB}+k_{AC})\right)$, and doing the analogous definitions for L_B and L_C, Eqs (22)–(24) can be written as Eqs (25)–(27).

$$-L_A\cdot M_{uvA} - (k_{BA}M_{uvB} + k_{CA}M_{uvC}) = i\cdot M_{zA}\cdot\omega_1 \tag{25}$$

$$-L_B \cdot M_{uvB} - (k_{AB} M_{uvA} + k_{CB} M_{uvC}) = i \cdot M_{zB} \cdot \omega_1 \tag{26}$$

$$-L_C \cdot M_{uvC} - (k_{BC} M_{uvB} + k_{AC} M_{uvA}) = i \cdot M_{zC} \cdot \omega_1 \tag{27}$$

The solution to this set of equations is Eq. (28).

$$M_{uvA} = \frac{i \cdot \omega_1 \cdot \left[M_{zA} \cdot \left(L_A \cdot L_B - k_{BC} \cdot k_{CB}\right) + M_{zB} \cdot \left(L_C \cdot k_{BA} + k_{BC} \cdot k_{CA}\right) + M_{zC} \cdot \left(L_B \cdot L_{CA} + k_{BA} \cdot k_{CB}\right)\right]}{-L_A \cdot L_B \cdot L_C + k_{BA} \cdot k_{CB} \cdot k_{AC} + k_{AB} \cdot k_{BC} + L_A \cdot k_{BC} \cdot k_{CB} + L_B \cdot k_{AC} \cdot k_{CA} + L_C \cdot k_{AB} \cdot k_{BA}} \tag{28}$$

This result is simplified by assuming equilibrium between all species ($1 = \frac{k_{AB} \cdot k_{BC} \cdot k_{CA}}{k_{AC} \cdot k_{CB} \cdot k_{BA}}$), and that M_{zA} is significantly larger than any other magnetisation term, such as is the case for water when looking at very dilute solutions of paramagnetic ions, and that direct exchange between species B and C can be ignored. By the same token, if M_{uv} is defined as sum of the magnetisation of species A, B and C, then the main contributor will be M_{uvA}. The imaginary part of M_{uv}, v, then becomes Eq. (29), which is reminiscent of a Lorentzian function, and as this is the absorptive component it describes the observed NMR signal.

$$v = \frac{-\omega_1 \cdot M_{zA} \cdot \left[\frac{1}{T_{2A}} + \sum_{j=B}^{C} \left\{ k_{Aj} \cdot \frac{\frac{1}{T_{2j}^2} + \frac{k_{jA}}{T_{2j}} + \Delta\omega_j^2}{\left(\frac{1}{T_{2j}} + k_{jA}\right)^2 + \Delta\omega_j^2} \right\} \right]_X}{\left[\frac{1}{T_{2A}} + \sum_{j=B}^{C} \left\{ k_{Aj} \cdot \frac{\frac{1}{T_{2j}^2} + \frac{k_{jA}}{T_{2j}} + \Delta\omega_j^2}{\left(\frac{1}{T_{2j}} + k_{jA}\right)^2 + \Delta\omega_j^2} \right\} \right]_Y^2 + \left[\Delta\omega_A + \sum_{j=B}^{C} \left\{ k_{Aj} \cdot \frac{k_{jA} \cdot \Delta\omega_j}{\left(\frac{1}{T_{2j}} + k_{jA}\right)^2 + \Delta\omega_j^2} \right\} \right]_Z^2} \tag{29}$$

The expression can be further simplified still by reasoning that if $\Delta\omega_j$ is very small it makes only a minor contribution to the expressions contained in brackets X and Y, and if $\Delta\omega_j$ is very large then the fractional change will be very small over the frequency range of a typical ^{17}O NMR signal, which is the case here. Either way, brackets X and Y become largely frequency independent, and the shape of the signal is mainly described by bracket Z.

The function v_A will then have maximum absolute amplitude when bracket Z approaches zero, as bracket Y is assumed to be constant, which renders $v_A = \left|\frac{-\omega_1 \cdot M_{zA}}{[\ldots]_Y}\right|$. By the same reasoning, the half-height, $\left|\frac{-\omega_1 \cdot M_{zA}}{2 \cdot [\ldots]_Y}\right|$, is obtained when brackets Y and Z in Eq. (29) are of equal value. The half-height is obtained at half the signal width, which can be experimentally

measured through determination of $\frac{1}{T_2}$ — in this case the half-width at half-max of the exchange-broadened water signal (as distinct from that of the pure water signal, $\frac{1}{T_{2A}}$). The expression for the half-width at half-max then becomes as shown in Eq. (30).

$$\frac{1}{T_2} = \frac{1}{T_{2A}} + \sum_{j=B}^{C} \left\{ k_{Aj} \cdot \frac{\frac{1}{T_{2j}^2} + \frac{k_{jA}}{T_{2j}} + \Delta\omega_j^2}{\left(\frac{1}{T_{2j}} + k_{jA}\right)^2 + \Delta\omega_j^2} \right\} \tag{30}$$

This equation is a key insight of the Swift and Connick method, since it provides an experimentally measurable quantity, the *excess* paramagnetic line width of the water signal, $\frac{1}{T_{2p}} = \frac{1}{T_2} - \frac{1}{T_{2A}}$, that is connected with the exchange kinetics of paramagnetic ions with water. This excess paramagnetic line width can be measured through two experiments—one of water which is not in exchange with a paramagnetic species, and one in which it is.

For a two-species system, e.g., where water is A and B is a paramagnetic metal aquocomplex, we can substitute m for B and w for A. As was done in Section 2.2 on the McConnell–Bloch equation, for steady-state situations, such as equilibria, $k_w = p_{wm} \cdot k_m$, where $p_{wm} = \frac{n[m]}{[w]}$ and n is the number of exchangeable water ligands per each paramagnetic ion. This reasoning leads to Eq. (31), where k_m is the desired unknown.

$$\frac{1}{T_{2p}} = p_{wm} \cdot k_m \frac{\frac{1}{T_2^2 m} + \frac{k_m}{T_{2m}} + \Delta\omega_m^2}{\left(\frac{1}{T_{2m}} + k_m\right)^2 + \Delta\omega_m^2} \tag{31}$$

Eq. (31) will approach $\frac{1}{T_{2p}} = p_{wm} \cdot k_m$ if (a) $\Delta\omega_m^2$ is much larger than $\frac{1}{T_{2m}}$, that is relaxation proceeds through a rapid change in the precessional frequency, or (b) if $\frac{k_m}{T_{2m}}$ is much larger than $\frac{1}{T_2^2 m}$, which is the case when paramagnetic relaxation is fast. In either case, the determination of the rate of exchange is straightforward. The issue, then, is knowing whether either of these two conditions is actually operating.

Since the temperature dependence of k_m in these two cases should follow the Eyring–Polanyi relationship, $k_m = \frac{k_B \cdot T}{h} \cdot e^{-\frac{\Delta H^\ddagger}{R \cdot T} + \frac{\Delta S^\ddagger}{T}}$, a plot of $\log_e\left(\frac{1}{T_{2p}}\right)$ vs $\frac{1}{T}$ should show a linear relationship.

The temperature region where this linear relationship is true varies with the chemical species, and may be outside of the liquid range of water, or may be very narrow. It is thus informative to consider the two remaining cases.

In the case where $k_m^2 \gg \Delta\omega_m^2 \gg \frac{k_m}{T_2^2 m}$, Eq. (31) approaches $\frac{1}{T_{2p}} = \frac{p_{wm} \cdot \Delta\omega_m^2}{k_m}$, that is chemical exchange is rapid, and the observed line width is controlled by the change in the precessional frequency.

In the case where $\frac{k_m}{T_{2m}} \gg \frac{1}{T_2^2 m}$, $\Delta\omega_m^2$, Eq. (31) approaches $\frac{1}{T_{2p}} = \frac{p_{wm}}{T_{2m}}$, that is the paramagnetic relaxation process dominates the line width.

In these latter cases the temperature effect on the different terms needs to be accounted, as shown in Eqs (32) and (33): [4]

$$\Delta\omega_m = \frac{2\pi g_L S(S+1) B_0}{3 k_B T} \left(\frac{A}{h}\right) \tag{32}$$

$$\frac{1}{T_{2m}} = \frac{4\pi^2}{3} S(S+1) \left(\frac{A}{h}\right) \left(\frac{1}{k_m + \frac{1}{T_{1e}}}\right) \tag{33}$$

S is the electron spin, g_L is the Landé factor, A/h is the hyperfine coupling constant, T_{1e} is the electron relaxation term and B_0 is the field strength.

A complicating issue is that g_L, A and T_{1e} often are unknown, in which case they are determined through fitting of the expanded Swift–Connick equation over a larger temperature range. Although this is a common approach—more common in the literature than simply restricting measurements to the range where $\frac{1}{T_{2p}} = p_{wm} \cdot k_m$—the number of variables that need to be determined is associated with the risk of introducing unacceptably large errors. Still, this has proven to be an effective approach in the past. The behaviour of the Swift–Connick approach under different limiting cases are summarised in Figs 1 and 2.

The shift of the water signal can also be used to aid in fitting, since implicit in the assumption that bracket Z is zero in Eq. (29), is that Eq. (34) holds:

$$\Delta\omega_A = -p_{wm} \cdot \frac{k_m^2 \cdot \Delta\omega_m}{\left(\frac{1}{T_{2m}} + k_m\right)^2 + \Delta\omega_m^2} \tag{34}$$

This gives a reduced chemical shift, $\Delta\omega_p = \dfrac{k_m^2 \cdot \Delta\omega_m}{\left(\dfrac{1}{T_{2m}} + k_m\right)^2 + \Delta\omega_m^2}$ which, like $\frac{1}{T_{2p}}$, was defined as the difference between the observed ^{17}O NMR signal of water in the presence, and absence, of a paramagnetic species, but scaled by division with p_{wm}. Maigut et al. [16] use a very similar form of Eq. (32), that incorporates outer-sphere ($\Delta\omega_{OS}$) contributions through Eq. (35), something which they do for $\frac{1}{T_{2p}}$ as well.

$$\Delta\omega_p = \frac{1}{p_{wm}}\left(\Delta\omega_{obs} - \Delta\omega_{ref}\right) = \frac{k_m^2 \cdot \Delta\omega_m}{\left(\dfrac{1}{T_{2m}} + k_m\right)^2 + \Delta\omega_m^2} + \Delta\omega_{OS} \tag{35}$$

Alternatively, in some cases where there are simple linear or exponential relationships which can be observed experimentally, but that lack rigorous interpretation. For example, the temperature dependence of T_{2m} and $\Delta\omega_m$ is, at times, determined by fitting to empirical equations but the parameters lack specific physical meaning. Likewise, in some cases the equations can be

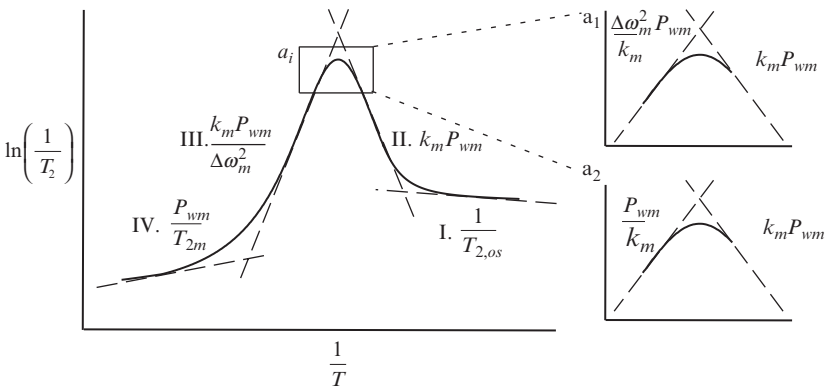

Fig. 1 The Swift–Connick equations allow one to use the temperature dependencies of experimental ^{17}O NMR line widths to estimate rate coefficients for ligand exchange reactions. Although the Swift–Connick equations are nonlinear, they have nearly linear regions where the major terms can be isolated. These linear regions are labelled Region I, II, III and IV in this figure. The *insets* labelled a_1 and a_2 in this figure show that the inversion in line widths can be due to two causes and should be interpreted with caution. The assumptions are discussed in the text and the approximations are detailed further in Fig. 2.

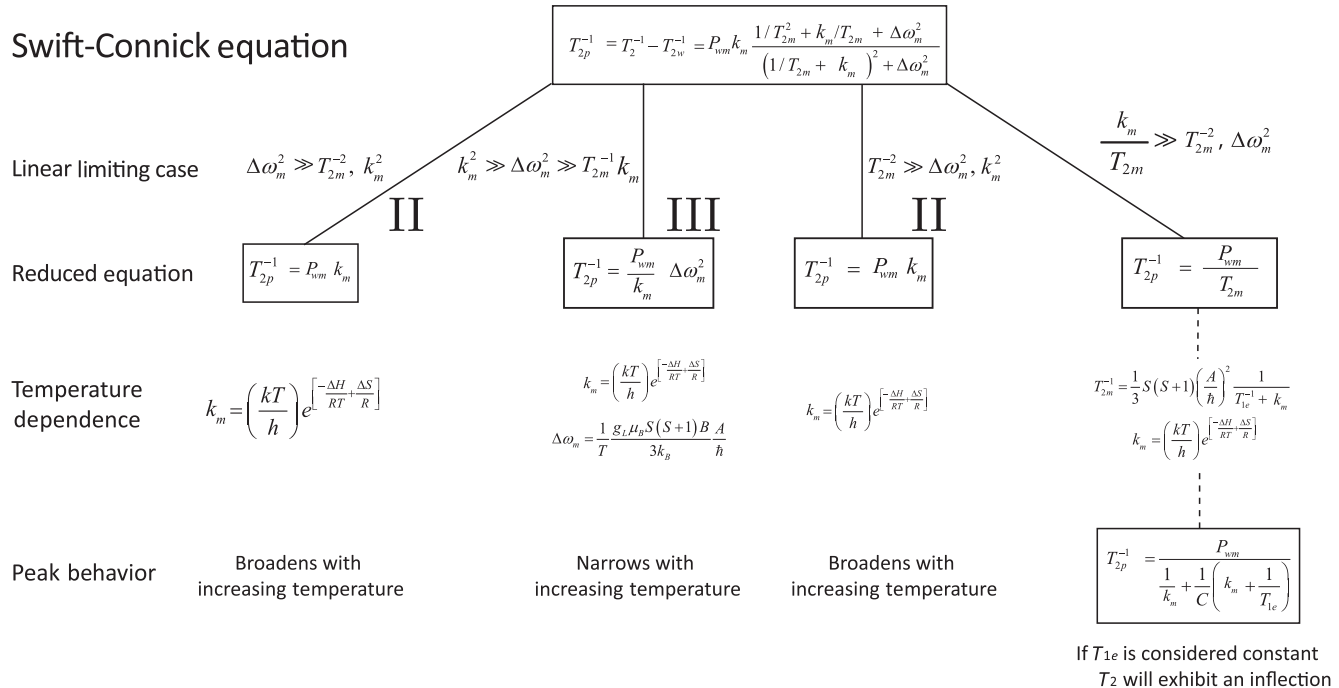

Fig. 2 The Swift–Connick equations are nonlinear but have linear regions where rate date for ligand exchange reactions can be estimated from the temperature dependencies of ^{17}O NMR spectra. The entire equation is shown at the *top outlined in a box*. The linear approximations are shown below, and the required physical conditions, with labels 'II' and 'III' corresponding to the regions identified in Fig. 1. The temperature dependencies of the key parameters are shown in the *next lower level* on the diagram and at the *bottom* of the figure is identified the key behaviour in ^{17}O NMR spectra with increases in temperature.

further simplified where, e.g., $\Delta\omega_m$ is comparatively small, as is the case with Mn(II) [16].

The Swift–Connick equation is based on a series of assumptions—dilute solutions, equilibrium, exchange that is fast enough relative to the transverse relaxation of the signal but slow relative to the duration of the applied pulse—and in its expanded form involves the determination of a large number of variables. In practice the judicious selection of reaction conditions and further simplification of the temperature dependence of the different parameters makes the determination of exchange kinetics using this approach relatively straightforward. It is essential, however, to remember that the exchange kinetics here are inferred and not directly measured.

3. SOLUTION DYNAMICS OF NANOMETER-SIZED AQUEOUS CLUSTER IONS

NMR spectroscopy, and ^{17}O NMR in particular, revolutionised polyoxometalate chemistry because it allowed scientists to clearly identify clusters that were stable in solution (see Fig. 3). The field of polyoxometalate chemistry really advanced in the early part of the 20th century with the establishment of the structures of tungstic acid and derivatives [17,18], but the work was heroic in the sense that the chemists relied heavily upon indirect evidence of cluster existence in solution (see Pope [19]).

The research that advanced the field proceeded in several clear stages. The first stage focused on structural chemistry, meaning mineralogy and X-ray structure determination. The earliest work actually came from the mineralogists, who identified decavanadate polyoxometalate clusters as essential to several minerals in uranium ore deposits [20]. In the first half of the 20th century, the field was dominated by X-ray crystallography, which continues in mineralogy as polyoxometalate clusters are discovered to form naturally [21–25] and as new clusters are identified [26–28] as minerals were attempted to be synthesised [29]. The mineralogists worked in parallel with polyoxometalate chemists who synthesised metal-substituted and lacunary clusters with specific functions in mind. New compounds are reported weekly and many are tailored for specific uses [30–41].

Beginning in the 1970s, aqueous solutions were prepared using NMR nuclei and spectra were collected. Because the coordination number of oxygen atoms in these clusters vary much more than the metals, ^{17}O NMR became a key tool in structural analysis [3,42–48] as the oxygen sites in different coordination environments were assigned to signals. In a typical

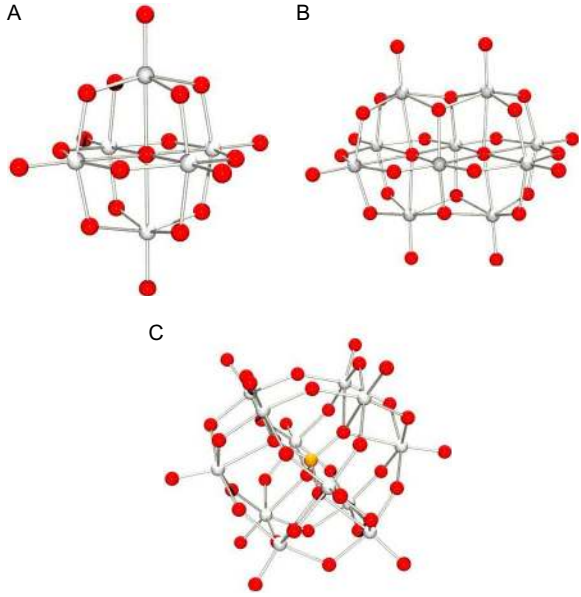

Fig. 3 Some examples of polyoxometalate ions that form stable solutions in water and contain a wide range of coordination environments for oxygen. (A) The Lindqvist ion $[Nb_6O_{19}]^{8-}$. (B) The decametalate ion $[Nb_{10}O_{28}]^{6-}$. (C) The Keggin ion $[SiNb_{12}O_{40}]^{16-}$. Niobium, oxygen and silicon atoms in *grey*, *red* and *gold*, respectively.

experiment, isotopically enriched polyoxometalate ions were dissolved into isotopically normal water if they were inert to isotopic substitution. Isotopically normal polyoxometalates were dissolved in pure ^{17}O-enriched solutions if they were labile and remade themselves quickly on the experimental timescale. ^{17}O NMR signals were clearly separated as more highly coordinated oxygen atoms appeared downfield, and sometimes far downfield, of the terminal waters and terminal hydroxyls. Farthest downfield were the terminal oxo-sites with multiple bonds to the metal. A good example is shown in Fig. 4 where the ^{17}O NMR signals for the decaniobate ion are assigned. This work on site assignment led to a considerable acceleration in the discovery and understanding of polyoxometalate ions, including substituted and lacunary forms. Targets could be synthesised, dissolved into a solvent and characterised quickly.

A second stage, overlapping with efforts in structural chemistry, was the use of NMR to establish the equilibria between metal ions and polyoxometalate clusters. Obviously the systems that were characterised had labile metals, such as the vanadate and molybdate systems [49–56], but the effects of substitutions, such as peroxo moieties for oxo moieties, could

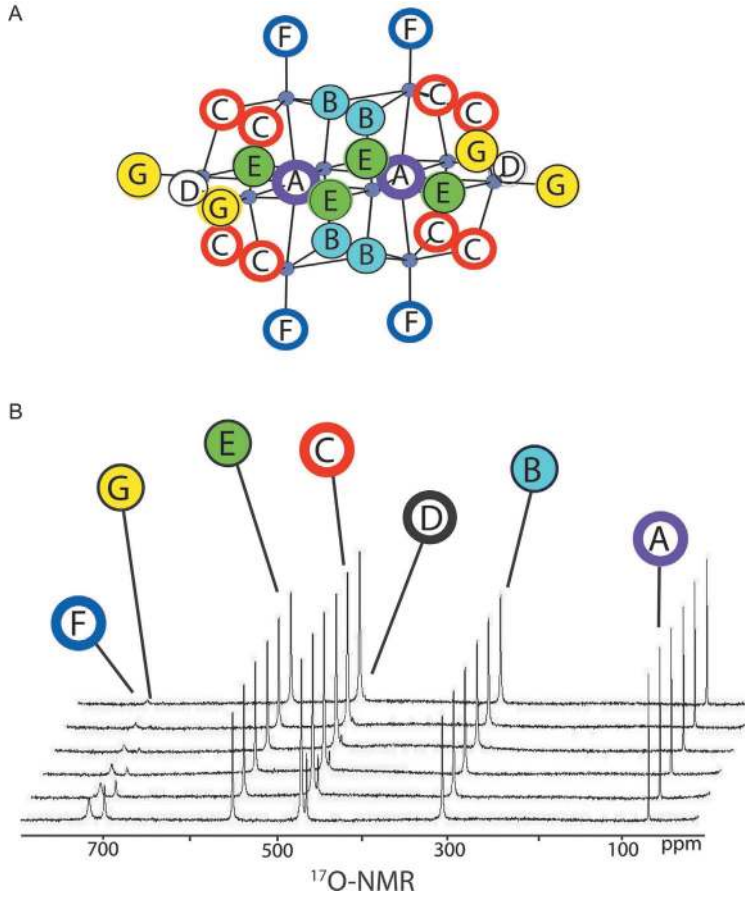

Fig. 4 (A) The $[H_xNb_{10}O_{28}]^{(6-x)-}$ ion has seven oxygen sites, here identified by *color*. (B) The oxygen sites give well-separated and distinct signals in a ^{17}O NMR spectrum of the dissolved ion. Note that some sites have ^{17}O NMR signals that diminish with time as those oxygen sites isotopically equilibrate with the isotopically normal bulk solution. The diminution of signal is particularly evident in the signals that are farthest downfield. *Adapted from E.M. Villa, C.A. Ohlin, E. Balogh, T.M. Anderson, M.D. Nyman, W.H. Casey, Reaction dynamics of the decaniobate ion $[H_xNb_{10}O_{28}]^{(6-x)-}$ in water, Angew. Chem., Int. Ed. 47 (2008) 4844–4846; see also W.G. Klemperer, K.A. Marek. An ^{17}O NMR study of hydrolyzed Nb^V in weakly acidic and basic aqueous solutions, Eur. J. Inorg. Chem. 2013 (2013) 1762–1771.*

be assessed directly by careful pH titrations coupled to NMR spectroscopy that showed the variations of key species. NMR spectroscopy, such as ^{51}V or ^{95}Mo, could be used to map the acid–base chemistry of the clusters and the dependence of equilibrium on total dissolved metal concentrations, which dominates much of the solution chemistry because of the nature of

multimeric equilibrium. Consider the reaction to assemble the Al_{13}^{7+} polyoxocation from solvated aluminum ions:

$$13Al^{3+}(aq) + 28H_2O(l) = \left[AlO_4Al_{12}(OH)_{24}(OH_2)\right]^{7+}(aq) + 32H^{+}(aq) \tag{36}$$

The equilibrium constant has the form: $K = \frac{\left(Al_{13}^{7+}\right)(H^{+})^{32}}{\left(Al^{3+}\right)^{13}}$, where the parentheses indicate thermodynamic activities. The key observation is that the concentration of the cluster ion ($Al_{13}^{7+} \equiv [AlO_4Al_{12}(OH)_{24}(OH_2)]^{7+}(aq)$) is exquisitely sensitive to the pH and the total dissolved metal ion concentration. The fact that proton concentration scales to the 32nd power, and aqueous aluminum ion concentration to the 13th power, means that the cluster appears and disappears with very slight changes in solution composition. Such chemistry is ideally suited for NMR spectroscopy where clear signals for the presence or absence of the cluster could be identified, and the reactions reversed. This literature is enormously valuable because it dispelled the idea that large clusters were only metastable, transient features.

A third stage arose when NMR spectroscopy was used to investigate the kinetics of reactions in the oxide substructures and functional groups of polyoxometalate ions in solution. For obvious reasons, again ^{17}O NMR spectroscopy was particularly useful although other NMR nuclei could be used in sufficiently simple reactions, such as isomerisation of isomers in tungstate ions [57,58] or electron self-exchange between two structurally similar polyoxometalates having identical stoichiometries [59] where the NMR signals of metals such as ^{27}Al can be followed to assess the reaction rates.

In discussing these kinetic studies it is useful to separately discuss rapid reactions, such as exchange of polyoxometalate-bound waters with bulk waters, which can proceed on submillisecond rates, from the slower reactions affecting bridging oxygen sites in the clusters. The traditional tools of ^{17}O NMR spectroscopy, as discussed in Section 2, can be immediately adapted to aqueous cluster chemistry as long as the larger size and slower tumbling of the ions is recognised. Swift–Connick methods of estimating rates of exchange of bound and bulk waters have been applied to the polyoxoaluminate cations [19,20,51–61], and to waters bound in the sandwich of a Wells–Dawson polyoxometalate ion [61–63]; these have metal hydroxide layers separating two tungstate clusters. In general, the reactivities of those bound waters are shown to react in ways that are broadly similar to

what is understood from the aquated ions [64,65]. The rates scale with structural charge, for example, and scale over many orders of magnitude with metal in the sandwich layer; waters bound to d^8 Ni(II), for example, exchange much slower than those bonded to d^5 Mn(II), whether or not they are in a cluster. The similarity led immediately to attempts to assign mechanisms of the water exchange reaction via high-pressure NMR, as discussed in this chapter.

Although there was active research in the kinetics of substitution reactions in these clusters before the advent of cheap ^{17}O NMR, the methods were much slower and involved, for example, ^{18}O—^{16}O substitutions followed by mass spectroscopy (e.g. see Ref. [66–68]). The interpretations were greatly enriched by NMR spectroscopy when site-specific sets of reactions could be followed easily [69].

The slower reactions of isotopic substitution into bridging oxygen atoms in these cluster ions can only be studied via ^{17}O NMR as for similar structures the rates can differ by many orders of magnitude. Various oxygen sites in the decaniobate ion, for example, take months to isotopically exchange with an aqueous solution [2,70,71], yet the structurally identical decavanadate ion reacts to completion in minutes [69].

The ^{17}O NMR spectroscopy has shown that, to a surprising degree, the rates of isotopic exchange in these large ions are regiospecific—different oxygen sites exhibit vastly different rates of exchange even though the clusters themselves are not dissociating. The two most comprehensive sets of studies involve the aluminate polyoxocations [60] and the decaniobate anions [2,71,72], where targeted metal substitutions could be used to change systematically the reactivities [73,74]. Coupling of NMR spectroscopy to molecular-dynamic simulations emphasises that pathways for isotopic exchange involve metastable, partly opened forms of the large cluster ions. Stated differently, the cluster ions constantly sample their energy landscape by relaxing into partly dissociated forms and interactions with counterions seem to be very important to the kinetics.

Isotopic exchange into the bridges proceeds via these open metastable structures but the molecules often do not fully dissociate and isotopically equilibrate with the aqueous solution. Thus, some sites can remain inert to exchange in the cluster ion as other sites equilibrate via vastly different rates but broadly similar pH dependencies. The identity of these metastable forms depends upon the structure, symmetry and composition of the stable polyoxometalate ion and various metastable structures interact with, and are stabilised by, counterions. Thus, rates of oxygen isotope exchange in various

sites in a nanometer-sized cluster ion depend upon solution composition. Recent activity, since 2011, in the field of ^{17}O NMR spectroscopy involving polyoxometalates and other relevant classes of molecules is reviewed later.

The key insight to reaction dynamics provided by these ^{17}O NMR studies is that dissociation of the structural metal oxide bridges in these nanometer-sized clusters is enormously complicated and counterintuitive. Pathways cannot be identified by simulation or by experiment alone but require both approaches conducted in tandem. In contrast, the rates of loss of a water molecule from these clusters fall into familiar ranges and seem to connect well to research on monomer ions.

The discovery of a potentially homogeneous water oxidation catalyst which is fully inorganic, that is lacking any organic moieties, in the form of $[Co_4(H_2O)_2(PW_9O_{34})]^{10-}$, raised the prospect of a new class of robust catalysts using first-row transition metals for one of the most important transformations at the moment [75]. To better understand the pH stability and exchange kinetics of the bound water ligands, two studies of $[Co_4(H_2O)_2(PW_9O_{34})]^{10-}$ were undertaken simultaneously and independently by Ohlin et al. [61] and Lieb et al. [63].

Ohlin et al. characterised $[Co_4(H_2O)_2(PW_9O_{34})]^{10-}$ and the structurally related but catalytically inactive molecule $[Co_4(H_2O)_2(P_2W_{15}O_{56})]^{16-}$ (see Fig. 5) by titrimetry, electrospray mass spectrometry and electron paramagnetic resonance (EPR) in order to elucidate the pH stability range and purity of the molecules in solution [61]. Given the paramagnetic nature of the Co(II) moieties, the rates of exchange of the bound water ligands were measured using the Swift and Connick approach described in Section 2.3. Since this approach to exchange kinetics requires that the solution composition is known with absolutely confidence, ruling out any presence of dissociated Co(II) from the dissolved polyoxometalate complexes was a particular concern. This exclusion was accomplished in part by using titrimetry coupled to spectroscopy to determine the pH range in which the compounds could be titrated reversibly, and by following the change in the excess charge of the cluster. Of particular interest was the use of perpendicular vs parallel polarisation EPR spectroscopy to detect dissociated Co(II) ions, as the cobalt centres in the molecules are ferromagnetically coupled, and any free, dissociated Co(II) ion would not be. It should be noted that the authors did find that the two polyoxotungstate molecules did undergo a two-proton protonation process with a pK_a of ca 4.5, but that this is likely to be associated with protonation of a site on the polyoxotungstate ligand,

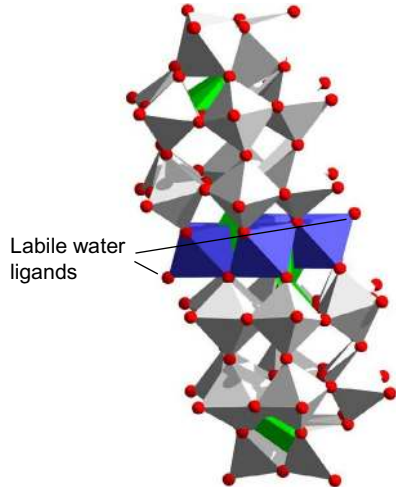

Fig. 5 Structure of the $[M_4(H_2O)_2(P_2W_{15}O_{56})_2]^{16-}$ ion (M = Mn(II), Co(II)), with the labile aqua ligand oxygen atoms indicated. Hydrogen atoms have been left out. Tungsten, oxygen, phosphorous and transition metal atoms given in *grey*, *red*, *green* and *blue*, respectively.

and not the aqua ligand bound to the cobalt site, as this is expected to have a pK_a of well above 8.

Swift–Connick ^{17}O NMR measurements of the exchange rates showed only minor pH dependence within pH 4.5–6.3, as would be expected given the generally high pK_a of water ligands bound to Co(II), and gave rates of exchange of the same order of magnitude to those found in the cobalt hexaaqua ion under similar conditions. The rates of exchange also varied very little between the two polyoxometalates, with rates of exchange of 1.5×10^6, 1.9×10^6 and 3.21×10^6 s^{-1} for $[Co_4(H_2O)_2(PW_9O_{34})]^{10-}$, $[Co_4(H_2O)_2(P_2W_{15}O_{56})]^{16-}$ and $[Co(H_2O)_6]^{2+}$ at pH 6.0, 6.3 and ca 1, respectively.

High-pressure ^{17}O NMR measurements of the rates of exchange allowed for the calculation of activation volumes, which were found to be positive but small (5.6 and 2.2 cm^3/mol for $[Co_4(H_2O)_2(PW_9O_{34})]^{10-}$ and $[Co_4(H_2O)_2(P_2W_{15}O_{56})]^{16-}$)—smaller than the activation volume of $[Co(H_2O)_6]^{2+}$ ion (6.2 cm^3/mol)—although it should be noted that any attempt to link activation volumes to reaction pathways is notoriously difficult for polyionic molecules in aqueous solution.

Lieb et al. studied the same $[Co_4(H_2O)_2(PW_9O_{34})]^{10-}$ polyoxotungstate complex as Ohlin et al., in addition to the catalytically inactive $[Co(H_2O)SiW_{11}O_{39}]^{6-}$ ion [63]. As in the preceding study the molecules were

characterised in solution using electrospray mass spectrometry, and rates of ligand exchange and activation volumes were determined using ^{17}O NMR spectroscopy and Swift–Connick formalism. However, Lieb et al. studied the molecules over a much larger pH range than Ohlin et al.—from pH 4.6 to 10.0—since the $[Co_4(H_2O)_2(PW_9O_{34})]^{10-}$ ion in catalytically inactive below pH 7, with a maximum turnover frequency observed at pH 8. Lieb et al. found that the rates of water ligand exchange on the $[Co_4(H_2O)_2(PW_9O_{34})]^{10-}$ ion varied little with pH, with a minimum of $1.50 \times 10^6\ s^{-1}$ at pH 6.0 and a maximum at pH 10.0 of $2.20 \times 10^6\ s^{-1}$. High-pressure ^{17}O NMR measurements gave a small, positive activation volume of 4.1 cm^3/mol.

Similarly, the rates of water ligand exchange on the $[Co(H_2O)SiW_{11}O_{39}]^{6-}$ ion showed little pH dependence between pH 6 and 10, but interestingly the rate of exchange was an order of magnitude lower than for the phosphotungstate complex. The activation volume was also found to be negative but small, at -1.5 cm^3/mol. Importantly, the authors found that both molecules were stable up to pH 10, whereas free $[Co(H_2O)_6]^{2+}$ is only stable under acidic and near-neutral conditions. Free Co(II) monomer, $[Co(H_2O)_6]^{2+}$ and hydrolysis products, could not have accounted for the observations.

Prompted by the lack of pH dependency of the rates of exchange on the $[Co_4(H_2O)_2(P_2W_{15}O_{56})]^{16-}$ ion, Sharma et al. studied the stability and rates of water ligand exchange on the structurally analogous $[Mn_4(H_2O)_2(P_2W_{15}O_{56})]^{16-}$ ion [62]. This molecule also exhibits a two-proton protonation process at pK_a ca 3.3–4.0, depending on method of determination, with the similarly in pK_a of this molecule and the cobalt analogue further supporting the locus of protonation as being situated on the polyoxotungstate ligand, which is identical for the two molecules.

Like Co(II), Mn(II) is also paramagnetic, and thus suitable for investigation using the Swift–Connick approach described earlier. In contrast with the $[Co_4(H_2O)_2(P_2W_{15}O_{56})]^{16-}$ ion, however, the rate of exchange $[Mn_4(H_2O)_2(P_2W_{15}O_{56})]^{16-}$ ion was found to be strongly dependent on the pH. While the rate of aqua ligand exchange on the $[Mn(H_2O)_6]^{2+}$ ion was found to vary very little with pH ($1.22 \times 10^7\ s^{-1}$ at pH 3.2 and $1.31 \times 10^7\ s^{-1}$ at pH 6.0), the rate of exchange of the aqua ligand on $[Mn_4(H_2O)_2(P_2W_{15}O_{56})]^{16-}$ increased 15-fold when decreasing the pH from 6.0 to 3.2. There was no indication that this was associated by decomposition of the molecule, as supported by titrimetric analysis which showed

that pH titration was reversible to ca pH 2.5. The locus of protonation remains to be determined, and is likely to be on the polyoxotungstate ligand, but in sufficient proximity to the bound aqua ligand that either electronic effects or intramolecular hydrogen bonding can play a role. The authors also left open the role that associative vs dissociative pathways may be influenced by protonation of the ligand, given that monomer ions of Co(II) generally exhibit dissociative mechanisms and those of Mn(II) take part in associative pathways.

In order to further attempt to provide an answer to the differences in behaviour of cobalt(II) and manganese(II) polyoxotungstates in terms of exchange, the same authors looked at a set of monomeric Mn(II) and Co(II) coordination complexes.

In spite of the resurgence of interest in first-row transition metal complexes with simple *N*-donor ligands such as phenanthroline and bipyridine, the rates of exchange of bound water ligands on many of these have until recently not been determined. Acharya et al. determined the rates of exchange of a series of 2,2′-bipyridyl and phenanthroline complexes of Co(II) and Mn(II) using the Swift–Connick approach described in Section 2.3 [76]. The study was complicated by the presence of dynamic equilibria in these systems, so that it is generally impossible to achieve solutions which are monospecific in any given species.

This complexity necessitated the calculation of speciation diagrammes for each system and set of conditions, so that the solution composition would be known with confidence at the conditions under which the rates of aqua ligand exchange were determined.

Rates determined by the Swift–Connick approach are inferred through a single observable property (the excess line width of the solvent signal). Because the presence of several paramagnetic species in exchange with the solvent will all contribute to this single observable property, a contributing complicating factor is that, even for species with the same paramagnetic centre, the individual contribution to the excess line width of the solvent signal will depend not only on such influences as the nature and number of nonexchanging ligands but also on the number of exchanging ligands. More directly, the contribution to the line width will scale directly with the number of exchanging ligands on the paramagnetic centre, so that higher concentrations of a $[M(H_2O)_2L_2]^{x+}$ species are needed than of a $[M(H_2O)_4L]^{x+}$ species to achieve the same observable broadening, even if the rates of exchange are identical. This difference makes the rates

of exchange more difficult to determine the fewer the number of exchangeable ligands are present in multicomponent solutions, such as those used in this study.

The authors found that the rates of exchange in the Mn(II) complexes scaled well with the Mn-OH_2 bond distance, with the rate of exchange increasing with decreasing bond distance. This scaling is interesting in light of the previous study of Sharma et al. which showed that the rate of exchange in a $[Mn_4(H_2O)_2(P_2W_{15}O_{56})]^{16-}$ ion increased with protonation, a process which shortens the Mn-OH_2 bond distance. For Co(II), however, no clear relationship between Co-OH_2 distances and rates of exchange was found, which is consistent with the lack of influence of protonation on the observed rates of exchange in the Co(II) polyoxotungstates.

Similarly, Co(II) showed little dependence on the number or type of ligands, with all systems showing rates of exchange within a narrow range of $1.6–3.1 \times 10^6\ s^{-1}$. In contrast, the Mn(II) complexes covered a slightly larger range, from 1.8 to $7.2 \times 10^7\ s^{-1}$.

Panasci et al. investigated the rates of exchange in an iron(III) tetramer with two bridging (hydr)oxo groups and four aqua ligands, $[Fe_4(\mu\text{-}OH)_2(hpdta)_2(H_2O)_4]$ (hpdta = 2-hydroxy-propane-1,3-diamino-*N*,*N*,*N*′,*N*′-tetraacetate) [77]. The molecule is diprotic, with two pK_a values of 5.7 and 8.8, respectively, where the lowest pK_a corresponds to the protonation of the hydroxo-bridge and was confirmed to be stable at pH below this pK_a and above pH 3, as determined by potentiometric and spectroscopic titrations.

The neutral charge, which minimises electrostatic and counterion effects, and the six-membered coordination environment, made this tetramer an interesting target to better understand iron-oxide mineral surfaces, as most discrete Fe(III) species are monomeric, heptacoordinate and charged and thus make poor analogues to the polymeric surfaces of minerals. As the iron(III) centre is paramagnetic, the rates of aqua ligand exchange could be measured by the methodology of Swift and Connick, including at high pressure in order to determine activation volumes (Fig. 6). The rate of water ligand exchange was found to be 10^4 times higher in the target molecule than in $[Fe(H_2O)_6]^{3+}$, but consistent with other iron complexes bound to aminocarboxylate ligands, with the rates of exchange generally correlating well with the Fe-OH_2 distance in this class of complexes (Fig. 7). Notably, the rate of exchange decreased with increasing pH, which was attributed to deprotonation of a bridging hydroxo moiety. As with the polyoxometalate sandwich complexes, rates of water exchanges from the tetramer seem to be

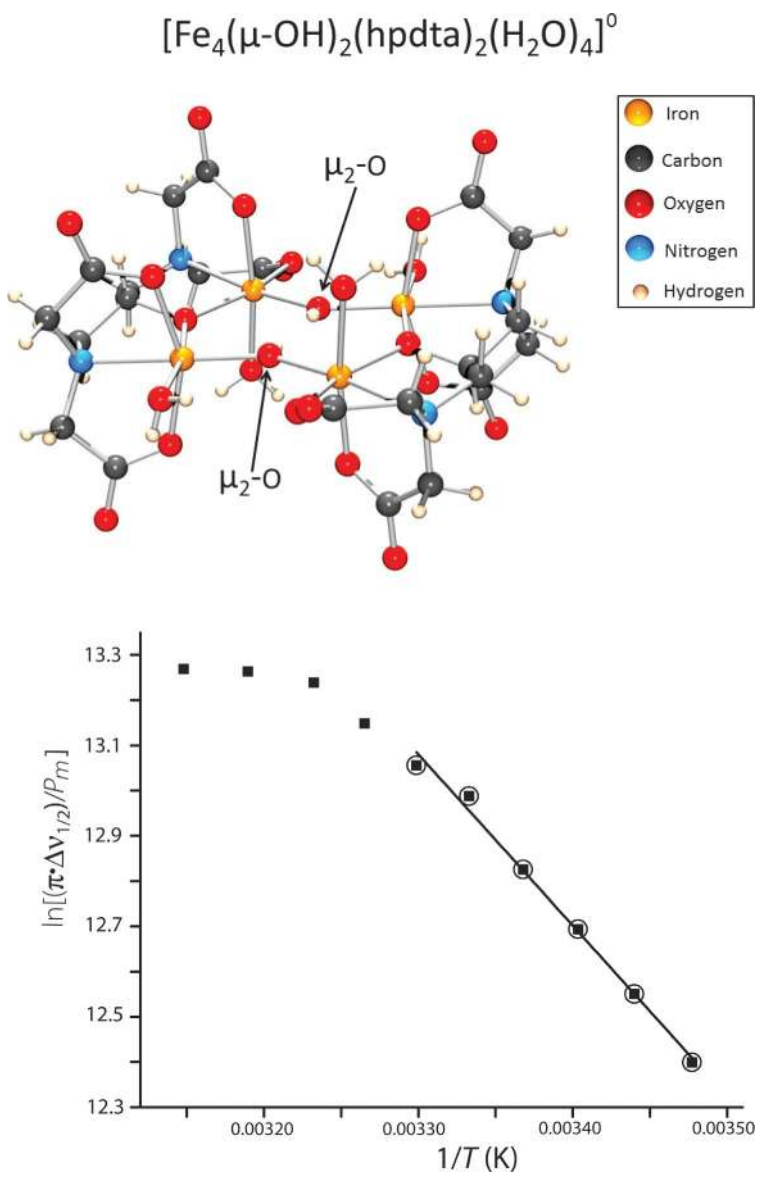

Fig. 6 (*Top*) The ferric tetramer ion ([Fe_4(μ-OH)$_2$(hpdta)$_2$(H_2O)$_4$] (hpdta = 2-hydroxypropane-1,3-diamino-*N*,*N*,*N*′,*N*′-tetraacetate)) captures some of the structural complexity that might exist at the surface of iron-hydroxide minerals, yet retains integrity in solution so that the rates of exchange of the bound and bulk waters can be measured using Swift–Connick methods. The ion has four metal centres and oxo bridges that protonate in near-neutral pH conditions. (*Bottom*) The ^{17}O data for bulk water signals in solutions containing the tetramer ion broaden relative to a solution without the paramagnetic ion. These data can be interpreted using the Swift–Connick model to yield kinetic data for water exchanges from the four sites on the [Fe_4(μ-OH)$_2$(hpdta)$_2$(H_2O)$_4$] ion. The *line* corresponds to that portion of the data used to estimate rate coefficients. $\Delta\nu_{1/2}$ is the half-width of the ^{17}O water signal.

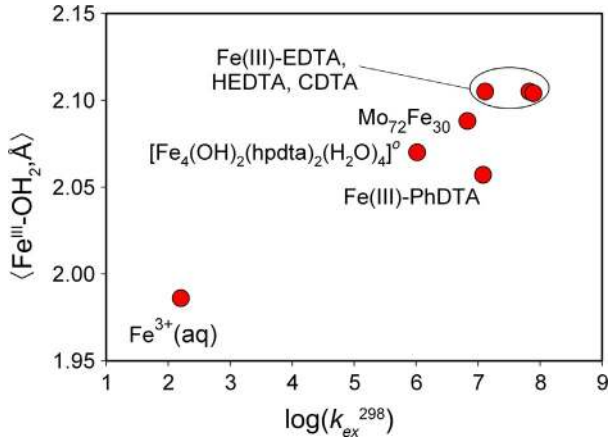

Fig. 7 The rate constant for exchange of water ligands bound to the $[Fe_4(\mu\text{-}OH)_2(hpdta)_2(H_2O)_4]$ ion is much larger than for the $[Fe(OH_2)_6]^{3+}$ ion but correlates well with other aminocarboxylate ferric complexes. The result suggests that water-exchange rates are affected most by broad chemical features such as overall charge and not details of the structure. *Adapted from A.F. Panasci, C.A. Ohlin, S.J. Harley, W.H. Casey, Rates of water exchange on the $[Fe_4(OH)_2(hpdta)_2(H_2O)_4]^0$ molecule and its implications for geochemistry, Inorg. Chem. 51 (2012) 6731–6738; ligand abbreviations are listed in that paper.*

consistent with the more extensive library of results for monomer complexes; these are apparently robust reactions that are not highly sensitive to small changes in structure.

The activation volume was small, 1.85 cm^3/mol, suggesting a dissociative interchange mechanism for the exchange. As the complex is neutral, counterion effects that are present in most of the preceding examples of activation volume determination would not be expected to be important here, although solvent rearrangement may still be important. The molecule is quite interesting because there are so few data on ligand exchange events in oxo-bridged iron clusters, particularly those with such an interesting protonation chemistry (Fig. 6) and neutral charge. The molecule is perhaps the best existing model for the complicated surface chemistry of iron-(hydr) oxide solid surfaces.

In addition to these studies there has been a wealth of work on Swift–Connick type ^{17}O NMR measurements on biological molecules and contrast agents, but which fall somewhat outside the scope of this review [78–108].

The polyoxoniobates are a class of polyoxometalates which were long ignored in favour of the polyoxovanadates, -tungstates and -molybdates.

In contrast with ^{51}V, ^{183}W and $^{95/97}$Mo, ^{93}Nb is not a practicably useful nucleus for NMR experiments, so ^{17}O NMR plays an even more important role in the understanding of the solution chemistry of this class of compounds.

Johnson et al. determined the rates of exchange of individual oxygen sites in a tetrasiliconiobate ion, $[H_{2+x}Si_4Nb_{16}O_{56}]^{(14-x)-}$ [109]. This study was part of a greater investigation of rates of oxygen exchange kinetics of structural oxygen sites by ^{17}O NMR in polyoxoniobates [2,72,110,111], but the number of distinct oxygen sites and the low symmetry presented particular problems with assigning observed ^{17}O NMR signals to oxygen sites. This challenge was solved using a computational approach and will be further described in Section 5. The general approach in these studies has been to enrich the polyoxoniobates in ^{17}O—either during synthesis or under hydrothermal conditions post synthesis—and then dissolving the enriched molecules in isotopically normal water and following the disappearance of the ^{17}O NMR signals over time as the structural oxygen sites exchange with the bulk water, with rates of exchange varying from hours to months. The structural integrity of the molecule during the exchange is confirmed by comparing the ^{17}O NMR signals of water bound to a signal area standard, $TbCl_3$, in an insert with the signal area of nonexchanging sites in the molecule. In contrast with many of polyoxoniobates molecules in the previous studies, the tetrasiliconiobate ion was found to be stable over a very wide range of pH, from pH 6–13.

Most of the ^{17}O NMR signal shifts did not show any pH dependence, which has generally been the case with most polyoxoniobates, with the notable exception of the hexaniobate ion, $[Nb_6O_{19}]^{8-}$. However, in the present ion a signal originating from an oxygen atom bridging an Si atom and an Nb atom was found to shift by ca 20 ppm when over the pH range studied. Even more dramatically, one signal corresponding to an oxygen atom connecting to niobium atoms was found to shift by almost 200 ppm between pH 6 and 10, and a range of other signals shifted by up to 40 ppm. The rates of exchange of the individual oxygen sites with the bulk water, in contrast, increased steadily with increasing pH, and there was little difference in the pH dependence of the rates of exchange of different oxygen sites, even when comparing the sites which corresponded to the signal that shifted by 200 ppm with sites that showed no pH-dependent chemical shift. As has been observed previously [2,72,110,112,113], while bridging oxygen sites are the *loci* of protonation, the sites which exchange the fastest are

generally the terminal oxygen sites, owing the reduced number of bonds and structural rearrangement needed to accommodate exchange.

The solution chemistry of even homoleptic isopolyoxoniobates is very poorly understood. The aqueous solution chemistry of polyoxoniobates is dominated by $[Nb_6O_{19}]^{8-}$ and $[Nb_{10}O_{28}]^{6-}$, and the latter converts readily and rapidly into the former at elevated pH, but there is no species known which can be used to construct a balanced reaction. Key to improving the understanding of this solution chemistry is ^{17}O NMR.

Klemperer and Marek studied the base-induced hydrolysis of the decaniobate ion, $[Nb_{10}O_{28}]^{6-}$, by ^{17}O NMR, changing the pH by acetate or phosphate buffers, or by tetramethylammonium or potassium hydroxide addition and following the solutions with time [70]. At elevated pH, in addition to observing the well-established conversion of $[Nb_{10}O_{28}]^{6-}$ into $[Nb_6O_{19}]^{8-}$, the authors also observed a transient intermediate, consistent with the previously from electrospray mass spectrometry [2] hypothesised $[Nb_7O_{22}]^{9-}$. The authors also observed that the dissociation of the decaniobate ion into hexaniobate could be reversed by heating for half an hour to an hour.

A previously isolated trimer of $[Nb_7O_{22}]^{9-}$ in which the units are linked by $[NbO(OH_2)]^{3+}$, $[Nb_{24}O_{72}]^{24-}$, was also observed in a narrow range of base added, which is the first time it has been observed by NMR. The study showed how careful control of the conditions of hydrolysis can be used to probe the chemistry of this class of compounds. This result is particularly important since a large proportion of published polyoxometalate and -niobate syntheses involve hydrothermal activation, conditions which do not lend themselves easily to in situ investigation, nor provide conditions which can be easily classified as subtle or mild.

Uranium, with the discovery of the uranyl (per)oxo clusters, has shown that it possesses a rich range of chemistry which is not that dissimilar from the classical polyoxometalates [28]. Harley et al. looked at the pressure-dependent rates of exchange of the –yl oxygen sites in the uranyl ion, $[UO_2(OH_2)_4]^{2-}$, with bulk water [13]. Here, the absence of a paramagnetic centre precludes Swift–Connick-type exchange kinetics, the fast exchange precludes preenrichment of the molecule as is done with the polyoxoniobates, and the distance between the ^{17}O NMR signal of the –yl oxygen, which is found at ca 1100 ppm, and the bulk signal water, which is the shift reference at 0 ppm, rules out direct coalescence studies.

Instead, the rate of exchange was determined through saturation transfer. A selective π pulse was applied bulk water signal, leading to an inversion of

the magnetisation. As the net magnetisation of the water oxygen site is now negative, exchange with the uranyl oxygen site leads to a decrease in the positive net magnetisation of the latter, leading to a decrease in the signal intensity on application of a broad $\pi/2$ observation pulse relative to a system which does not undergo exchange. By varying the interpulse delay—the mixing time—data were obtained which was fitted to an equation derived from the McConnell–Bloch equations discussed in Section 2.2. By performing these experiments over a range of pressure activation volumes for different conditions could be determined. The activation volumes varied little with uranyl or hydroxide concentration, and were in the -9 to -10 cm^3/mol range, suggesting a mechanism with some associative character, although caution should be taken when interpreting data from reactions involving coordinating solvents and ions because of the influence of electrostriction, which is discussed later in the context of high-pressure NMR and the pressure-dependent dielectric constant of water. The mechanisms of ligand exchange reactions can be unambiguously interpreted from activation volumes only if the complexes are homoleptic and uncharged, which is not the case for oxo site exchanges since these sites presumably must protonate to exchange with bulk waters.

Maksimovskaya et al. identified for the first time a novel borotungstate polyoxometalate, $[H_3BW_{13}O_{46}]^{8-}$, in solution together with the protonated lacunary ion $[HBW_{11}O_{39}]^{8-}$ using multinuclear NMR methods, including ^{17}O NMR [114]. Detailed analysis of the ^{183}W NMR spectrum was used to determine the isomeric form of the protonated lacunary ion, while ^{17}O NMR showed the proton to be delocalised between two sites based on shifting of the corresponding NMR signals to lower frequencies due to protonation-induced lengthening of the W—O distances. Furthermore, NMR was used to explore solutions prepared under different conditions and revealed methods for synthesising purer solutions of both molecules.

An intermediate complex in the conversion of $[H_3BW_{13}O_{46}]^{8-}$ into $H_5[BW_{12}O_{40}]$ was also identified by ^{183}W and ^{17}O NMR, $[BW_{11}O_{39}WO_2]^{7-}$, suggesting a mechanism for this conversion. Identification of this intermediate is significant, as where there is a wealth of solid-state information about different classes of polyoxometalates, there is a relative dearth of detail regarding solution behaviour and very little direct information indeed regarding mechanisms of conversion.

Kandasamy et al. investigated a novel tin-substituted polyoxotungstate, $[(MeO)SnW_5O_{18}]^{3-}$, by ^{1}H, ^{17}O, ^{115}Sn and ^{183}W NMR [115]. Key to the

preparation was ^{115}Sn NMR which was used to follow the formation of the target molecule, whereas ^{17}O and ^{183}W were the main tools in characterising the product in solution. The authors enriched the molecule in ^{17}O using ^{17}O-enriched water added to the acetonitrile solvent and noted that they had found that oxygen sites bridging a heterometal and a tungstates atom generally yielded stronger ^{17}O signals than oxygen sites bridging two tungsten atoms when the compounds were enriched in this way, presumably owing to the inertness of the latter type of oxygen sites.

Coyle et al. reported a series of polyoxomolybdates formed from protonolysis of $[(iPrO)TiMo_5O_{18}]^{3-}$ [116]. ^{17}O NMR was used to characterise the molecules in solution and revealed the relative basicities of the complexes, which was attributed to the electron donating ability of the heteroatom-ligand unit. As in the previous study, the relative intensities of the ^{17}O W–O–W signals were used to assign the signals.

O'Halloran et al. used ^{17}O NMR as part of an attempt to settle the nature of some Pt-, Pd- and Au-containing polyoxometalate complexes that had been reported in the literature, and which were remarkable in having M═O moieties (M = Pt, Pd or Au), something which is generally not expected for these metals [117]. While distinguishing between electron-rich atoms can be challenging by X-ray crystallography in disordered complexes, NMR methods are nuclei specific and can play a role in resolving questions about polyoxometalate structures. The authors, by enriching a polyoxotungstate ligand with ^{17}O, were able to correct an earlier assignment of a ^{17}O NMR signal to Au═O and found that it belongs to a W═O signal in a decomposition product instead. Similarly, a signal assigned to Pd═O was found to correspond to an oxygen bridging between Pd and tungsten in a decomposition product.

Ultimately, the Pt- and Au complexes were found to contain neither Pt or Au, whereas the Pd complex was confirmed to contain Pd, but the structure was found to be different. This work was significant in that, by reexamining cases which had been found to be breaking a previously accepted rule, the Oxo Wall rule, the rule regarding the occurrence of M═O units among the transition metals was found to be upheld.

4. HIGH-PRESSURE NMR

4.1 Mechanisms of Ligand Exchange via ^{17}O NMR

As is evident in the previous section, nuclear magnetic resonance, and particularly ^{17}O NMR [118], has become a central tool for understanding aqueous solution dynamics. NMR is sensitive to motions that span from

nanosecond nuclear reorientations to isotope exchange reactions taking months. One particularly fruitful area of research was to establish the rates of exchange of solvation waters from around octahedral metal complexes. Rates of solvent exchanges are known to span a range of ca 10^{20}, largely through ^{17}O NMR studies of trivalent and divalent metals in water. The lifetimes scale from subnanoseconds, such as the La^{3+} ion where nearly every collision with the solvent leads to an exchange event, to $[Ir(OH_2)_6]^{3+}$, which exchanges a solvation water with the bulk once every two centuries at ambient conditions [119]. We do not review that work here because this subject has been well covered [64,65].

Knowing these rates of exchange of a solvation water is important because they indirectly yield the rates of other ligand exchange processes that proceed via Eigen–Wilkins pathways. Eigen–Wilkins pathways are processes where the first step is rapid formation of an electrostatic ion pair and the slower step is a subsequent displacement of an inner-sphere water from the solvation shell of the metal [120–122]. The first step proceeds to equilibrium. Research has shown that the rates of the second step, movement of a solvation water, are largely unaffected by the incoming ligand. Thus, measurements of rates of water exchange, coupled to use of the Eigen–Fuoss equation for estimating equilibrium constants for outer-sphere ion-pair formation, allow one to estimate a wide range of second-order rate coefficients [120–122]. Water exchange events from solvation shells to the bulk were elementary, or near-elementary reactions and high-pressure NMR could probe the activated state.

Furthermore, the change in rates with increases in pressure help one understand the *mechanism* of the reaction at the elementary scale—mechanism in this case means the extent that the incoming solvent molecule affects the transition state. When an aqueous solution is placed under pressure, Nature generally responds by packing water molecules more efficiently and waters that are bonded to the metal in the first solvation shell are packed more efficiently than bulk waters. Thus, solvent exchange reactions that have a considerable *associative* character, meaning that the coordination number *increases* in the transition, are enhanced by increases in pressure as a bulk water is transferred to the solvation sphere with a loss of net volume. Correspondingly, reactions with a considerable *dissociative* character, meaning a decrease in the coordination number in a transition state, are suppressed by increases in pressure because an inner-sphere water is transferred to the bulk. Mechanisms of most water exchange reactions fall intermediate between these two extreme cases, but high-pressure NMR over a range of 0.001–0.25 GPa plays a central role and this subject has been reviewed

several times [123,124]. There are, however, new devices being built to extend the work.

4.2 Devices to Reach GPa Pressures for Solution NMR

New efforts are underway to expand the pressure ranges for solution NMR well beyond the 0.001–0.25 GPa employed in ligand exchange kinetics, to 3.5–4.0 GPa. These pressures in the Earth are realised below the deepest part of the Earth's crust, or over 40 km depths. These efforts are now motivated to evaluate models of solution equilibrium developed by geochemists, which calculate solute activities and the equilibrium constants for a wide range of aqueous reactions [125–132]. The HKF model is among the most widely used ('HKF' from 'Helgeson, Kirkham and Flowers') and employs as one key variable the static dielectric constant of water at elevated temperatures and pressures [13,14,34–42,120–134].

Until recently, the conditions where the HKF model could be used were limited to temperatures less than 1000°C and pressures less than 0.5 GPa because these were the limits of experimental measurements of the static dielectric constant of water. In 2013, however, molecular-dynamic simulations were used to estimate the dielectric constant to 1200°C and 5 GPa [130,131]. These new conditions motivated scientists to design new NMR probes to reach GPa pressures and that are suitable for solution spectroscopy [135–138]. Additionally, there are separate very promising efforts to establish chemical-shift accuracy in defective diamonds using optical detection [139]. This technology is not yet sufficiently mature for standard solution NMR because the resolution is usually inadequate to resolve close chemical shifts, but promises a future technology for solution NMR at GPa pressures, albeit on a subnanoliter-sized sample volume.

New considerations must enter the interpretation of NMR spectra at these pressures that can be ignored in conventional studies at 0.2–0.4 GPa. For example, the dielectric constant for water reaches values over 100 at GPa pressures (Fig. 8), and the changes are profoundly nonlinear at $P < 1.0$ GPa. GPa pressures thus favour the separation of charges, leading to a large volume contribution to the activated equilibrium that arises from electrostatic forces, called *electrostriction*, which we mentioned in Section 3 when discussing the interpretation of activation volumes. The electrostriction volume is not linear with pressure, as can be seen by differentiating the Born solvation energy, $V_{el.} = \frac{-N_a(ze)^2}{8\pi\varepsilon_o e^2 r}\left(\frac{d\varepsilon}{dP}\right)$, and evaluating it with measured values of the dielectric constant using the static dielectric constant

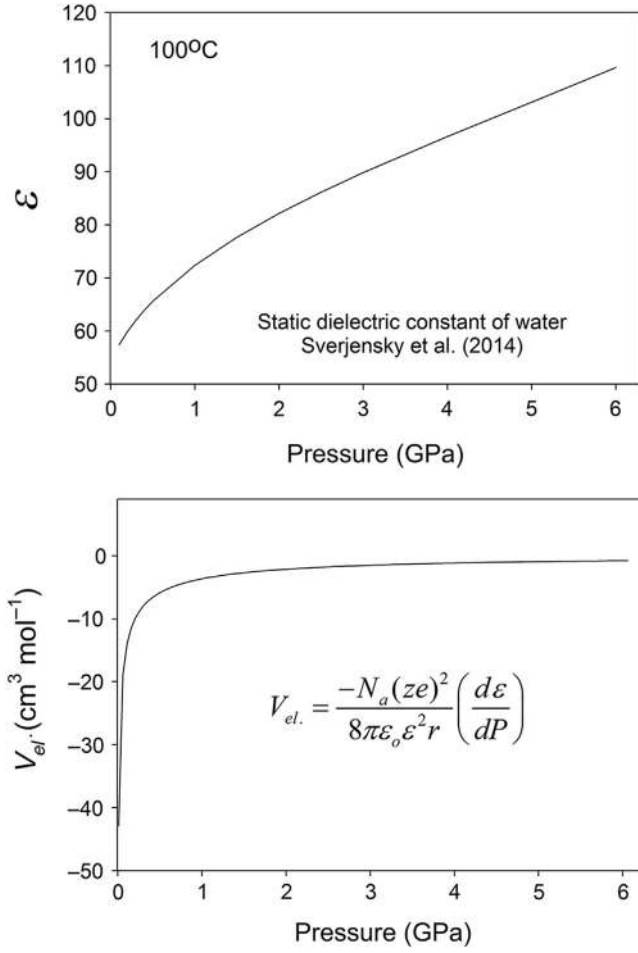

Fig. 8 (*Top*) The static dielectric constant of water at 298 K estimated to 6.0 GPa at 100° C from the data of Sverjensky et al. [131]. (*Bottom*) The pressure derivative of the Born equation yields the electrostriction volume, which here is similarly calculated for a $z = +2$ ion with a radius of 1.4 nm. Note that the electrostriction volume is large and variable, and arises from changes in the dielectric constant with pressure. Rapid changes in the electrostriction volume are observed at low pressures but diminish rapidly with increased pressure to become approximately constant beyond ca 1.0 GPa.

regression to 6.0 GPa [131]. Note that the contribution is large and variable at low pressures, just where traditional ^{17}O NMR experiments were conducted (Fig. 8).

The fact that the electrostriction volume becomes nearly constant at $P > 1.0$ GPa (Fig. 8) means that pressure-driven changes in chemistry, such

as changes in coordination number, solvation or bonding, can be better studied at high pressures than low. Contributions to the volume from the changing dielectric constant are minimal at very high pressures.

Changes in solution equilibria with GPa pressures are not small. Water dissociates more completely and the dissociation constants of oxyacids also change in parallel with the changing dissociation constant of water. Thus, weak acids like acetic acid become strong acids at elevated pressures. For example, a 0.05-M acetate/acetic acid solution that is happily buffered to pH 4.7 at ambient pressures drops to $pH < 1.5$ at 1 GPa. These changes in Brønsted acid–base strength make identification of a chemical-shift standard difficult if they are affected by hydrogen bonding. Reactions that depend upon protonation states of the complex, such as the tungstate sandwich molecules or the $[Fe_4(\mu\text{-}OH)_2(hpdta)_2(H_2O)_4]$ ion [62,77], have a contribution to the measured activation volumes that arise from the volume of water dissociation and protonation.

Another challenge to the interpretation of solution NMR spectra arises from the increased solution viscosities at GPa pressures. The hydrogen-bonding structure of water is considerably modified at these extreme pressures, leading to increased viscosities which are of course affected by any electrolytes dissolved into the solution [140]. In the "extreme narrowing" limit, the longitudinal relaxation rates of quadrupolar nuclei ($I > ½$) can be determined from Eq. (37),

$$\frac{1}{T_{1Q}} = \frac{1}{T_{2Q}} = \frac{3}{10}\pi^2 \frac{2I+3}{I^2(2I-1)} \langle \chi^2 \rangle \tau_c \tag{37}$$

where I is the spin of the nucleus, τ_c is the reorientation time of the molecule and $\langle \chi^2 \rangle$ is the mean square of the zero-average quadrupolar-coupling constant. The reorientation time of the molecule, τ_c, depends upon solution viscosity and can be related to a measureable diffusion coefficient using the Stokes–Einstein equation (Eq. 38),

$$D = \frac{kT}{6\pi\eta r} \tag{38}$$

where D is the self-diffusion coefficient of molecules in the solvent, r is the hydrodynamic radius of the molecule and all other variables retain their usual definitions.

Ochoa, Colla, Klavins, Augustine and Casey [137] built upon the extensive work by Jonas [141–146] to show that consistent results of solute diffusion could be achieved by using the clamp-cell and microcoil design

and they then extended the measurements to 1.9 GPa. They used NMR-measured diffusion coefficients to estimate viscosities at pressure via the Stokes–Einstein equation. They found that the apparent viscosities could be increased by a factor of ca 4 over the pressure range of 0.5–2.0 GPa in CsCl solutions. Greater increases were observed in $LaCl_3$ solutions.

Increased viscosities become important for interpreting NMR spectra at GPa pressures. The increased viscosity contributes directly to broader NMR line widths by slowing molecular tumbling, even in the absence of chemical causes such as enhanced rates of chemical exchange. Although pressure-enhanced increases in viscosity can usually be ignored for aqueous solutions in the 0.2–0.4 GPa range (but not in organic solvents [147]) [40–42,44–48,131,134–140,145–149], increased viscosities in the pressure range 0.5–2.0 GPa causes significant broadening of an NMR line width. This broadening must be accounted in interpreting ^{17}O NMR spectra to yield rates of reactions, or changes in equilibrium constants (Fig. 9). The increases in viscosity that they observed, if misinterpreted to be due to reaction volumes, would account for a -3 cm^3/mol apparent volume of reaction.

The original NMR probes that are used for high-pressure solution NMR derived from the pioneering work of Jonas [145,148,150], who build large-volume NMR probes to reach 0.5 GPa. These probes require wide-bore magnets. A separate commercial design uses sapphire NMR tubes to reach ca 0.2 GPa and a standard superconducting narrow-bore magnet,

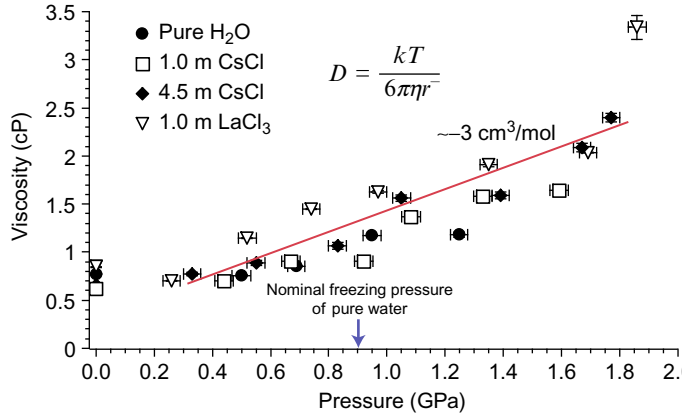

Fig. 9 Viscosities of aqueous solutions estimated from the measured diffusion coefficient of water in aqueous CsCl solutions and the Stokes–Einstein relation. The viscosity of water increases by a factor of ca 4 in the range 0.5–2.0 GPa [137]. If the resulting line broadening was misinterpreted as indicating a reaction volume, the result would be a -3 cm^3/mol error.

but in the last 5 years a third design was conceived by adapting a microcoil and NMR circuit to the clamp cells of solid-state physics. These new microcoil-based NMR probes extended the pressure range to ca 3–4 GPa at ambient temperatures [135,138]. With some changes in alloys, it should be possible to heat these probes to ca 500°C, although these temperatures have not been reached yet.

One of the first discoveries when using these new NMR probes is that the presence of electrolyte can easily double the freezing pressure of water or D_2O [136,137], from 0.9 to 2.0 GPa for $LaCl_3$ solutions. There are two apparent causes: (i) the electrolyte enhances the freezing pressure by normal colligative processes, and (ii) the freezing of solution into the high-pressure ices (Ice VI, VII) is slow on the NMR timescale, so that one can collect NMR spectra on solutions that are considerably super-pressured.

As NMR spectroscopists extend their work to these high pressures, one of the challenges that they will confront is assignment of chemical shifts. Internal standards will only be useful if their chemical shifts are not sensitive to the changing solution properties, such as the hydrogen-bonding networks as any shift standard than has Brønsted acid–base chemistry, for example, will vary wildly in chemical shift with pressure. Thus, the efforts in building high-pressure ^{17}O NMR probes, and application to cluster ions, are coupled to work to calculate chemical shifts from first principles, which is reviewed in Section 5.

5. COMPUTATION OF ^{17}O CHEMICAL SHIFTS OF METAL OXIDE CLUSTERS BY DENSITY FUNCTIONAL THEORY

In small, symmetric compounds the assignment of NMR signals to the correct site is often straightforward. This is not the case, however, in larger molecules with low symmetry, where there may be a large number of signals from atoms in similar sites and of similar abundance. Here signal assignment can be very challenging, and nearly impossible using only empirical tools. The difficulties in the case of ^{17}O NMR are compounded by the rapid relaxation rates of ^{17}O nuclei, which make difficult or impossible the two-dimensional NMR experiments that could help resolve signal overlap and assignments. Computational chemistry has an important role to play here. We will not be covering the computation of spin–spin coupling constants and electric-field gradients, although these are also of considerable interest.

The computation of NMR shielding constants involves modelling of the interaction of wave functions with a magnetic field rather than an electric one and presents a specific set of challenges.

The chemical shift, σ, arises because nuclei are surrounded by moving electrons which react to the presence of a magnetic field $\vec{B}_0$, and induce an opposing field, which is typically six orders of magnitude smaller. This induced field shields the nucleus and is proportional to $\vec{B}_0$ by σ, and the field actually experienced by the nucleus is $\vec{B}$, which is defined by Eq. (39); σ can be positive or negative.

$$\left|\vec{B}\right| = \left|\vec{B}_0\right| \cdot (1 - \sigma) \tag{39}$$

In order to calculate the shielding, all that remains to be computed is the magnitude of the induced field, and this is what is sought to be done using quantum chemistry programs. This is, however, not trivial. A detailed examination of how this is done is beyond the scope of this chapter and is available in the literature [151,152]. We will here only be discussing some of the key concepts and issues.

The shielding σ tensor is often written as the sum of the diamagnetic (σ_d) and paramagnetic components (σ_p), $\sigma = \sigma_d + \sigma_p$ [153], although it can be expanded to include relativistic spin–orbit coupling contributions (σ_{SO}) as well, $\sigma = \sigma_d + \sigma_p + \sigma_{SO}$.

The chemical shift δ is then the shielding compared to an agreed-upon reference signal, $\delta = \frac{\sigma_{ref} - \sigma}{1 - \sigma_{ref}} \times 10^6$, and is given in ppm.

The shielding has both isotropic and anisotropic contributions (Eq. 40).

$$\sigma = \sigma_{iso} + \sigma_{aniso} \tag{40}$$

With the exception of nuclei with low electron densities and small chemical shift windows, such as ^{1}H, the anisotropic shift is generally less important as it is typically much smaller—on the order of a few ppm. Compared with the chemical shift window of ^{17}O, which exceeds 2000 ppm, this is generally negligible.

While the diamagnetic component depends only on the molecular electronic ground state, accurate determination of the paramagnetic component requires knowledge of the complete set of unoccupied orbitals as it depends on excited singlet states, which is computationally challenging.

A compounding issue is that of the gauge-origin problem, where gauge-origin dependence leads to the potential issue of the choice of origin for the

coordinate system in the computations; changing the origin changes the calculated value. A popular enduring solution to this has been the gauge-independent atomic orbital (GIAO) method (sometimes also referred to as the gauge-including atomic orbital method), which originated with attempts to understand currents in aromatic systems, well before NMR was developed as an analytical technique [154].

The GIAO method can be used in conjunction with, e.g., DFT, perturbation theory, such as MP2, or coupled-cluster theory methods, such as CCSD(T). However, computing accurate chemical shifts of even small molecules such as carbon monoxide has proven to be challenging using either DFT or perturbation methods such as MP2 [155].

Correlated methods, while potentially highly accurate, are limited to very small systems due to their computational cost. Because of this, DFT is the most appealing method as it is now computationally cheap enough to allow for the use of large basis sets and sophisticated methods for even large inorganic molecules.

In terms of basis sets, larger is generally better, although some studies have found that smaller basis sets give better shift predictions than larger ones. One may speculate that this is primarily due to fortuitous cancellation of errors in these cases. Either way, since basis sets with effective core potentials (ECP), where some of the core atomic orbitals have been replaced by a potential, are popular in computational polyoxometalate chemistry, care needs to be taken to use all-electron basis sets in the computation of NMR shifts, at least on the nuclei for which shifts are being computed. For oxygen this is not generally a problem, but ECP basis sets such as LANL2DZ and def2-tzvp apply ECPs to atoms heavier than neon and krypton, respectively, which means that elements which are common in discrete metal oxide clusters such as Nb, Mo, Ta and W are all likely to require the use of ECPs. Some packages, such as the Amsterdam Density Functional computational software, provide all-electron basis sets for these elements too.

Because DFT does not inherently provide an explicit way of computing the electron exchange and correlation effects as a function of density, it necessitates the use of an exchange-correlation (XC) functional. Because there is no one 'true' XC functional, this needs to be carefully chosen for the task at hand—some XC functionals are better at providing realistic geometries, whereas others are more suited for other tasks.

Current XC functionals can be divided into a few main classes: local density approximations, generalised gradient approximations (GGA), and

hybrid functionals. Most functionals that are used today are either GGA functionals such as PBE and BP86, also known as pure DFT functionals, or hybrid functionals such as PBE0 and B3LYP, where a certain amount—typically 20%–30%—of exact Hartree–Fock (HF) exchange is used to replace the local exchange in order to treat nonlocal self-interaction better, but at increased computational cost.

While early work showed that the diamagnetic tensor was insensitive to the XC functional, the paramagnetic component depends strongly on it [152].

The paramagnetic component depends on computing accurate energy levels for both occupied and unoccupied molecular orbitals (MO). However, the computation of accurate MO levels using DFT is a significant challenge as most XC functionals strongly upshift some MO levels, while shifting other orbital levels less [156]. As a consequence, while many XC functionals can predict accurate relative MO levels for valence orbitals and even HOMO–LUMO gaps, getting accurate relative MO levels between other sets of MOs, such as between valence orbitals and higher-energy unoccupied orbitals, is very challenging. The development of the statistical average of orbital potentials (SAOP) XC, which is only implemented in the proprietary Amsterdam Functional package, was done with the intention of providing more accurate excitation energies using time-dependent DFT [157], but this particular functional has also seen use in the prediction of NMR shifts [158,159].

A practical issue is that of protonation. In many cases the protonation states of the discrete metal oxide clusters are simply not known in solution, let alone the corresponding pK_a values. While computational methods offer a route towards improving the understanding of protonation events in metal oxide clusters through the prediction of chemical shifts as a function of such events, it complicates the development of strategies for computing chemical shifts since the influence of the pH is not known or understood.

The focus of this section is on the prediction of ^{17}O NMR shifts in discrete metal oxide clusters such as polyoxometalates, but it is instructive to also look at the computation of shifts of other important NMR-active nuclei that are relevant to this class of compounds. In particular, ^{31}P, ^{51}V and ^{183}W are important here because the interpretation of ^{17}O NMR results for clusters is usually coupled to interpretation of spectra of the heavier nuclei. Much of the work has been done using the Amsterdam Density Functional package, which is due to a few factors, such as the predominance of a few

research groups in this field that are users of this package, the better ability in general of Slater-type orbitals at describing the electron density near the nucleus, and the easy availability of all-electron basis sets for even heavy transition metal atoms. Limitations in this package, such as historically limited implementations of XC functionals, have probably also affected the scope of some of the studies.

Phosphorous is, by definition, present only in heteropolyoxometalates, but this class includes some of the earliest known polyoxometalates, the heteropoly acids, such as the Baker–Figgis–Keggin and Dawson clusters. ^{31}P has abundance close to 100%, a spin of ½ and comparatively slow T_1 relaxation, which makes it a powerful tool for resolving solution dynamics via NMR. From the point of view of computation of chemical shifts, it also has the advantage of being found relatively early in the periodic table and so there is a range of potential all-electron basis sets available, but the disadvantage that the chemical shifts found in polyoxometalates typically only cover 10–20 ppm, out of a spectral window of 500 ppm. The exceptions are polyoxometalates functionalised with paramagnetic species that may yield ^{31}P signals that are shifted to well over 1000 ppm [61], but DFT struggles in general with paramagnetic materials and is known to fail even in providing accurate relative energetics of different spin states of the same molecule [160]. A particular feature of ^{31}P NMR is that the shift reference is a solution of a specific concentration, 85% H_3PO_4 in water, which can be difficult to reproduce experimentally, although there are strategies to address this [161].

Pascual-Borràs et al. have performed a systematic investigation of the computation of ^{31}P shifts in polyoxometalates and focused on a series of Keggin and Dawson polyoxotungstate and -molybdate ions and derivatives [162]. Using the Amsterdam Density Functional (ADF) package [163], which employs Slater-type orbitals that should describe the electron density at the nucleus better than Gaussian-type orbitals do, the authors explored different combinations of triple- and quadruple zeta basis (TZ and QZ) sets with single (P) or double polarisation functions (2P), in conjunction with GGA and hybrid XC functionals and taking into account relativistic effects through spin–orbit coupling. All of these calculations employed all-electron basis sets.

They found that a triple-zeta basis set with double polarisation functions (TZ2P) was sufficient for geometry optimisation, but that the situation was more complex for the computation of the ^{31}P NMR shift of the optimised structure. In general a triple-zeta double polarised (TZ2P) basis set would

give slightly more accurate results, but at double the computational cost of using the singly polarised TZP basis set.

Only GGA functionals, viz. OPBE, PBE and KT2, were investigated during optimisation, but both GGA and hybrid functionals were tested in the computation of the NMR shift. Here, PBE was an anomaly in that the results became much less accurate with the largest basis set (QZ4P). The popular B3LYP functional provided conspicuously poor predictions. Overall, the most accurate results were obtained for specific combinations of optimisation vs NMR computation methods, e.g., using PBE/TZ2P to compute shifts for the geometry obtained at OPBE/TZ2P, suggesting that—beyond using large basis sets and good quality functionals in general—an important factor in obtaining a good prediction is error cancellation. A compounding factor here is also the narrow range of the shifts of the molecules used in the study, which makes it difficult to further differentiate the effect of different functional and basis set combinations.

Vanadium yields a large family of polyoxometalates in the form of polyoxovanadates. Polyoxovanadates are typically synthesised from soluble metavanadate salts by adjusting the pH or the addition of addenda atoms. ^{51}V is an attractive nucleus since it has a large isotopic abundance (99.75%) and a large chemical shift window, and, despite having a spin of 7/2, the signals are comparatively narrow. The ^{50}V isotope, in contrast, is rarely used in spite of also being NMR active, due to its low abundance and broader signals.

Not surprisingly, ^{51}V has long been used to improve the understanding of polyoxovanadate solution dynamics. In contrast, ^{51}V chemical shift prediction is notoriously difficult. To our knowledge there has been no systematic and comprehensive effort to predict ^{51}V chemical shifts in polyoxovanadates, but the literature does contain a few isolated examples.

Vankova et al. explored the SAOP and BP (BP86) functionals as implemented in the ADF package together with different combinations of double- and triple-zeta basis sets and relativistic corrections through the zeroth-order regular approximation (ZORA) and spin–orbit coupling, and implicit solvation through the conductor-like screening model (COSMO) [158]. For the molecule investigated, $[PtV_9O_{28}]^{5-}$, use of SAOP in the NMR computation for the BP-optimised molecule gave a mean absolute error of 12 ppm for the four signals, but failed to predict the relative order of two of them. Izarova et al. used the same approach to compute the ^{51}V NMR signal shifts of $[PdV_6O_{24}(OH)_2]^{6-}$ and found that in order to get accurate predictions the introduction of 6–7 counterions was

required, with the best results obtained when both counterions and a single proton were introduced [159]. The authors concluded that this suggested that the ion pairing observed for the solid state structure was essentially maintained in solution, a point that is experimentally verified for some polyoxoanions [164].

Crucially, the essential role that counterions play in solution of these large ions suggests that detailed knowledge of the environment of the cluster is needed for accurate predictions, which has obvious implications relating to the prediction of NMR signal shifts for novel materials, such as those hypothesised in studies of solution dynamics.

^{183}W is an attractive nucleus given the rich chemistry of polyoxotungstates, including their use as ligands in reactions such as water oxidation catalysis [75]. In addition, the polyoxotungstates are more prevalent than any other class of polyoxometalate, and being able to observe the signals of framework tungsten atoms is thus of considerable interest. While ^{183}W has a spin of ½, a large shift window—spanning ca 8000 ppm—and is isotopically abundant (>14%), it has low sensitivity, which coupled with a long T_1 reduces its usefulness somewhat. The low resonance frequency also requires probes that can operate at under these conditions, which is normally not part of the standard NMR instrumentation set-up. Polyoxotungstates also tend to be inert to oxygen isotope exchanges, so that one can confidently assign the ^{17}O NMR signals to sites in the molecule.

Gracia et al. explored the computational prediction of ^{183}W shifts in two studies, with the first one focussing on ground state geometries, and the second one on molecules in reduced oxidation states. Here, a diverse collection of isopoly- and heteropolyoxotungstates were investigated. As in most of these studies, the Amsterdam Density Functional package was used, in conjunction with triple-zeta basis sets and the BP (BP86) functional, and ZORA. However, no implicit solvation was used, which may together with the use of a GGA functional have contributed to the observation that optimised structures had bond distances in excess of those found in the corresponding X-ray crystal structures.

The authors generally found a fair correlation between predicted and observed shifts for the ground state geometries [165]. While linear regression yielded an r^2 of 0.98, the slope was 0.79 and the intercept −10.27 ppm, so that the predicted distance between the signals is different from the observed one. This discrepancy is likely because, in spite of the structural diversity and the very large chemical shift window of ^{183}W, the shifts of tungsten nuclei in polyoxotungstates are predominantly found in a relatively narrow window between −200 and 300 ppm, with a particular concentration of shifts in the

−150 to −100 ppm region. The uneven distribution of recorded chemical shifts will affect the linear correlation. This sampling problem is a general issue with most such studies, as few systems will provide an even spread of observed signals. In the present case, the correlation is distinctly less accurate in the region where most of the signals are found, while it is more accurate for the extremes of the chemical shift window.

Either way, while the diamagnetic contribution was found to be relatively constant throughout the test series, the paramagnetic factor was the determining term in the predicted shift.

Gracia et al. also looked at reduced polyoxotungstates [166]. Here, the accuracy of the predicted shifts was generally lower than for the fully oxidised structures, but the computations reproduced the general trends well. Their study illustrated how changes in computed and observed NMR chemical shifts upon reduction could be used to describe localisation and delocalisation of electrons in reduced species. Interestingly, linear regression gave a slope of 1.21 and an intercept of −66 ppm, which is notably different from the corresponding parameters for the preceding study of fully oxidised polyoxotungstates. The negative intercept was interpreted as resulting from overestimated bond lengths.

Vilà-Nadal et al. predicted the ^{183}W shifts in a large and diverse set of heteropolyoxotungstates using ADF [167]. The authors obtained the best results, in terms of smallest mean absolute errors, when the geometries were optimised at BP86/QZ4P with implicit solvation through COSMO, and the shift computations were carried out at BP6/TZP with relativistic corrections through spin–orbit coupling and ZORA. In particular, accurate structures were found to be key to achieving good accuracies in the computation of shielding constants, and the authors discussed issues relating to asymmetry when using structures obtained from X-ray diffraction. No other XC functional was investigated. As in previous studies, most of the experimental shifts of the test compounds were found in a narrow region of −120 to −80 ppm, owing to the dominance O–W–O units in polyoxometalate structures. As will be demonstrated later with respect to ^{17}O NMR shift prediction, the accuracy of the predicted shift can depend strongly on the immediate coordination environment of the nucleus, i.e., a method may, for example, give a good prediction for a bridging unit, but not for a terminal one. Oxygen is different to the preceding elements in that it is present in all metal oxides by definition and it is abundant, as it is a framework atom. Thus, there are generally more distinct oxygen environments in any given discrete metal oxide cluster than for any other element, which makes ^{17}O arguably the most potentially important nucleus in this field of chemistry.

Consider as an illustration the example of the simple rock-salt solid, MgO (periclase). An interface between periclase and water exposes oxygens that differ in coordination number to Mg(II) from one to five, and six-coordinated oxygens are buried in the bulk material. In contrast, the Mg(II) metals at the interface are uniformly coordinated to six oxygen atoms. Thus, oxygens and ^{17}O NMR potentially contain the most information about structure.

In addition, as is clear from the brief overview given of the other main NMR-active nuclei in polyoxometalates, there is no nucleus which is simultaneously abundant, sensitive and for which it is straightforward to predict the NMR shifts. ^{17}O NMR thus has a central role to play in understanding the solution chemistry of metal oxide clusters.

Although organic chemists have not relied upon ^{17}O NMR as much as the inorganic oxide chemists, Wilson et al. explored the failure of DFT methods to accurately predict in particular the chemical shift of ^{17}O in even small organic molecules and derived a new exchange correlation functional which yielded much improved shielding constants for their test set [168,169]. In brief, the exchange correlation functional is based on the B3LYP functional, but uses 5% instead of 20% exact HF exchange in determining the Kohn–Sham orbitals, and turns off the use of HF exchange in the computation of the shielding constants. The resulting functional was named $B3LYP^{0.05}_{GGA}$. Using this approach the gas phase isotopic shielding constant of ^{17}O in CO was improved from −81.0 ppm (B3LYP with the Huzinaga IV basis set, HIV) to −40.0 ppm ($B3LYP^{0.05}_{GGA}$/HIV), which is considerably closer to the experimental value of -36.7 ± 17.2 ppm, and was an improvement on the CCSD(T) value of −52.9 ppm [170].

This functional has seen limited use in the ensuing decade and a half, perhaps owing to it only being implemented as a standard functional in a single piece of computational software, PQS, where it is supplied as the 'WAH' functional [171]. Nonetheless, a recent application of the WAH functional was in the computation at WAH/def2-svp of ^{17}O NMR chemical shifts of a large tetrasiliconiobate ion, $[H_{2+x}Si_4Nb_{16}O_{56}]^{(14-x)-}$, where it was used to assign signals in a low-symmetry polyoxometalate that could not have been easily assigned in any other way [109]. Importantly, the authors used the signal assignments to suggest the protonation state, as well as explain in part the observed pH dependency of the signals of the oxygen sites in the molecule. However, the computed shielding constants deviated significantly from the observed chemical shifts, suggesting that the WAH functional may not be as successful in predicting chemical shifts in discrete metal oxide compounds.

Early work on ^{17}O NMR shift calculations in metal oxide monomers, $[MO_4]^{q-}$ (M = W(VI), Mo(VI), Cr(VI), Re(VII), Tc(VII), Mn(VII), Os(VIII) and Ru(VIII)), by Kaupp et al. using ACESII [172] compared HF, DFT—using mainly the GGA functionals PW91 and BP86—and MP2 with and without accounting for relativistic effects [173]. They found that electron correlation became increasingly important in more deshielded systems where paramagnetic contributions are large, which led to failures by both MP2 and HF methods in predicting accurate ^{17}O shifts, with MP2 overestimating the chemical shift and HF underestimating it. For the highly deshielded RuO_4 oxygen sites, DFT using the BP86 functional gave a predicted shift of −765 ppm, whereas HF and MP2 predicted −3300 and 8262 ppm, respectively, whereas the experimentally observed shift is ca −815 to −828 ppm. In contrast, for the more shielded oxygen sites in $[WO_4]^{2-}$ DFT, HF and MP2 gave shifts of −157, −194 and −21 ppm, respectively. Here the experimentally obtained shift is −129 ppm. Consistent with the observations for HF, hybrid functionals, such as B3PW91, were found to perform increasingly poorly for increasingly deshielded systems with larger paramagnetic contributions, although the effect was not as dramatic as for HF.

Both Kaupp et al. and contemporary work by Schreckenbach et al. [174] using ADF explored the importance of relativistic effects. Relativistic effects cause contraction of the M–O distances and change the electronic structure, leading to increased shielding, and—while smaller for 3*d* and 4*d* elements—become increasingly important for heavier elements with 5*d* orbitals. The differences in chemistry of identical Nb(V) and Ta(V) oxides, for example, are attributed to relativistic contributions to Ta—O bonding.

Gracia et al. looked at the prediction of ^{17}O signal shifts in a series of hetero- and isopolyoxotungstates, which first necessitated a critical evaluation of the assignment of experimentally observed NMR signals [165]. Computations were carried out with ADF at BP86/TZP on geometries optimised at the same level of theory and included relativistic corrections through ZORA. For the test set, linear regression yielded a slope of 1.1 and an intercept of −66 ppm, with r^2 of 0.98, indicating that the method accurately reproduced the separation of the NMR signals, but overestimated the shifts by 66 ppm. The paramagnetic shielding was broken down into components, and the importance of each component for different types of oxygen sites was analysed. In particular, occupied-occupied MO coupling (the s-term) was found to vary in importance relative to the occupied-virtual MO coupling (the u-term), for different orders of oxygen coordination

environments. Whereas the s-term only gave a 5% contribution relative to the u-term for terminal oxygen sites, the contribution was 30% or more for more highly coordinated oxygen sites, such as the central μ_6-O in $[W_6O_{19}]^{2-}$. Notably, while the computational method in some cases failed to give the correct order of the predicted signals for ^{183}W, this was not the case for the ^{17}O shifts.

Gracia et al. also examined reduced polyoxotungstates, again using ADF [166]. While the focus in this study was on the ^{183}W signal shifts, the authors found that the computations reproduced the negative shift of all the oxygen sites in the molecules upon reduction.

Pascual-Borràs et al. investigated the computation of solution-phase shielding constants of a series of mainly Lindqvist-type polyoxometalate (POM) clusters [175]. These Lindqvist-type POMs have several types of structural oxygen atoms, including terminal η-O, and bridging μ_2-O and μ_6-O oxygen sites (where the subscript indicates the number of metal atoms to which the oxygen atom is bound), and which exhibit a wide range of chemical shifts. For example, while the experimental chemical shift in acetonitrile of the μ_6-O in $[W_6O_{19}]^{2-}$ is −80 ppm, the chemical shift of the terminal η-O is 775 ppm. This wide range makes this class of POMs a good test set for efforts to compute shielding constants. The authors explored a range of pure DFT or hybrid exchange correlation functional and triple- and quadruple-zeta basis set combinations using the ADF package which implements Slater-type orbitals. These functionals and basis sets describe the electron density better at the atomic nucleus than do Gaussian-type orbitals. In addition, scalar-relativistic corrections via ZORA was used to account for spin–orbit contributions.

The authors found that the pure DFT functionals OPBE and PBE performed better than the hybrid functionals, giving computed chemical shifts that were particularly close to observed shifts for the terminal η-O sites, while being off by 50 ppm or more for the more highly coordinated oxygen sites. This discrepancy is particularly interesting in light of the observations of Wilson et al., that not including exact HF exchange in the computation of shielding constants gave the most accurate shift for the oxygen in the CO molecule—an oxygen site which bears some resemblance to a terminal η-O in that the bond order is higher than one.

The authors also explored the effect of protonation using the polyprotic $[V_{10}O_{28}]^{6-}$ ion as an illustrative test case. A particular challenge is that the number of possible protonation sites is large, with several sites likely to be protonated at the same time, with protons being highly mobile on the NMR timescale. In addition, solutions may not be monospecific, so in order

to reproduce the observed chemical shift, a speciation diagram needs to be used to combine the computed shift of several different species to compute the overall observable shift. Using a multisite approach, Pascual-Borràs et al. found that the model that best described the protonation state at pH 4.5 was one which combined two $[HV_{10}O_{28}]^{5-}$ molecules—one which had a μ_3-O site protonated and one which had a μ_2-site protonated. These were combined in a 60:40 ratio to yield a shift that approached the experimental one. This is also a picture which is consistent with the one found based on X-ray crystallography [176]. Although Pascual-Borràs et al. found that applying linear regression improved the predicted chemical shifts, the different levels of accuracy in the computation of the shielding constants of different types of oxygen sites using pure DFT functionals means that this does not provide an ideal solution.

With this in mind, Sharma et al. reinvestigated the computation of ^{17}O NMR chemical shifts of a large range of structurally and chemically heterogeneous set of POMs [177] and used the Gaussian package for the computations [178], which uses gaussian-type orbitals. The authors focused on a series of decaniobates, $[M_xNb_{10-x}O_{28}]^{(x+6)-}$ (M = Ti, $x = 0$–2), in developing their method, as this class of polyoxometalates does not appreciably protonate in solution, and thus eliminating one potential source of error.

The authors found that, as in previous studies, pure DFT functionals such as OPBE gave fairly accurate shielding constants for terminal oxygen sites, but poor predictions for more highly coordinated oxygen atoms. By varying the amount of exact HF exchange in the PBE functional, they found that as the amount of exact HF exchange increased, the accuracy of the computed shift of the more highly coordinated μ_6-O sites improved, and those of the terminal η-O sites deteriorated. At 25% HF exchange, the error for all oxygen sites was approximately equal, allowing for effective application of linear regression. Conveniently, the well-established exchange-correlation functional PBE0 contains 25% HF exchange, and this functional was found to give both accurately optimised structures and accurate linearly regressed chemical shifts.

The authors developed a method which employed PBE0 and cc-pvtz for all oxygen sites, and LANL2DZ for all metal sites, during geometry optimisation, and PBE0/def2-tzvp in the GIAO computation of the NMR shifts. Shifts were computed and fitted against a test set including 209 ^{17}O NMR signals from 37 polyoxometalate ions to yield scaling factors. A regressed slope close 1.0 was obtained, which shows that the approach gives accurate separation of signals, with the main computed error being the relative chemical shift as compared to bulk water. This result is important, as it means that

the method is likely to have potential in resolving mixtures of compounds, in addition to simply assigning signals in monospecific solutions.

The Lindqvist ion of niobium, $[Nb_6O_{19}]^{8-}$, is known to be at least triprotic, with the pK_a values having been determined and the location of the protons known to be the μ_2-oxygen sites. Furthermore, the pH-dependent chemical shifts are known, including their temperature dependence. This made it a good test case for the computation of chemical shifts as a function of protonation. Sharma et al. found that by selecting the lowest energy isomer for each protonation state and by combining the contribution to the chemical shift of each protonated species according to the speciation diagram, the observed pH-dependent shift behaviour could be reproduced successfully.

These latter computations of the pH-dependent NMR shifts required the optimisation of all possible protonation geometries, and comparison of the energies. For the triply protonated hexaniobate ion, this necessitates the optimisation of 22 structures, even if geometries which include protonated terminal η-oxygen sites are excluded. For larger and less symmetric molecules the number of geometries that need to be considered quickly becomes forbiddingly large, in particular when more expensive computational methods are used. Yet, the corollary of the success in computing the pH-induced chemical shift variation is that in order to test or develop computational methods for predicting chemical shifts of different nuclei, it is absolutely necessary to know the protonation states (and possibly the counterion positions). As information about these are largely missing from the experimental literature, the onus is on both computational and experimental researchers in the field to collaborate in expanding the literature of DFT-based NMR shift predictions.

6. CONCLUSIONS

In this review we focused on the application of ^{17}O NMR to the solution dynamics of nanometer-sized discrete metal oxide clusters, which is a field of great interest to researchers in heterogeneous catalysis and geochemistry alike. In these fields the use of discrete and soluble fragments of metal oxides affords the possibility of providing detailed understanding of how this type of material behaves. Furthermore, the link between oxide surface chemistry in water and the chemistry of large aqueous oxide ions is explicit [179]. That in particular ^{17}O NMR is important here is a consequence not

only of the central role that oxygen plays in oxides but is also a testament to the importance of water as a solvent in catalysis and nature.

While ^{17}O NMR as a structural probe has long been understood to be important in this field, it is its use as a tool in understanding reactivities of metal oxide clusters that precipitated the writing of this chapter. A happy consequence of the general lack of scalar coupling in the ^{17}O NMR spectra of these types of systems is that the classical vector model of the Bloch equations is often sufficient to model dynamic phenomena in solution when probed by ^{17}O NMR, and the authors of this review believe that this is a level of theory which is considerably more accessible than models based on quantum mechanics. That the original papers by McConnell [11] and Swift and Connick [15] still receive 30–35 and 15–20 citations per year in spite of being published in 1958 and 1962, respectively, is a testament to this and is the reason why a large section of the review has been devoted to this.

A particular subdiscipline of ^{17}O NMR is high-pressure NMR, where recent advances in probe design have made heteronuclear NMR experiments accessible at pressures that are found below the bottom of the Earth's crust. Correspondingly high-pressure experiments inform extreme catalytic conditions, and which we review together with the application of high-pressure NMR in the determination of activation volumes. There is a world of new ^{17}O NMR chemistry to explore at these GPa pressures.

Advances in improving the sensitivity of NMR instrumentation have also made ^{17}O NMR more accessible, and isotopic enrichment is not strictly necessary for a large range of systems. As increasingly complex systems are being investigated by ^{17}O NMR, signal assignment is also increasing in complexity. Computational methods show promise here, but as is so often the case, a balance has to be struck between level of theory and computational cost, and accuracy. For the type of nanometer-sized discrete metal oxide clusters which are the focus of this review, DFT is the most promising approach. In spite of recent advances in the computation and prediction of ^{17}O NMR chemical shifts, achieving acceptable accuracy for the types of systems is still a significant challenge. This challenge may not be fully met even by the advent of new exchange-correlation functionals, but may instead have to rely on Moore's law and advances in computer speed.

The authors hope that this review will encourage more chemists to incorporate ^{17}O NMR techniques—and in particular dynamic ^{17}O NMR techniques—into their toolbox, as it is a versatile nucleus of an element which has such a central role in nature.

AUTHOR CONTRIBUTIONS

C.A.O. has mainly written Sections 1, 2 and 5 and overseen the work. W.H.C. has mainly written Section 4. The authors have contributed equally to Section 3. All authors approve and share responsibility for the whole chapter. Work by W.H.C. is supported by the Department of Energy Office of Basic Energy Sciences via Grant DE-FG02-05ER15693.

REFERENCES

[1] R.K. Harris, E.D. Becker, S.M. Cabral de Menezes, R. Goodfellow, P. Granger, NMR nomenclature: nuclear spin properties and conventions for chemical shifts. IUPAC recommendations 2001. International Union of Pure and Applied Chemistry. Physical chemistry division. Commission on molecular structure and spectroscopy, Magn. Reson. Chem. 40 (2002) 489–505.
[2] E.M. Villa, C.A. Ohlin, E. Balogh, T.M. Anderson, M.D. Nyman, W.H. Casey, Reaction dynamics of the decaniobate ion $[H_xNb_{10}O_{28}]^{(6-x)-}$ in water, Angew. Chem. Int. Ed. 47 (2008) 4844–4846.
[3] W.G. Klemperer, 17O-NMR spectroscopy as a structural probe, Angew. Chem. Int. Ed. 17 (1978) 246–254.
[4] S.J. Harley, C.A. Ohlin, W.H. Casey, Geochemical kinetics via the Swift-Connick equations and solution NMR, Geochim. Cosmochim. Acta 75 (2011) 3711–3725.
[5] F. Bloch, Nuclear induction, Phys. Ther. Rev. 70 (1946) 460–474.
[6] See https://se.mathworks.com/products/matlab.html.
[7] See https://www.gnu.org/software/octave/.
[8] See https://www.wolfram.com/mathematica/.
[9] See https://www.maplesoft.com/.
[10] See http://maxima.sourceforge.net/.
[11] H.M. McConnell, Reaction rates by nuclear magnetic resonance, J. Chem. Phys. 28 (1958) 430–431.
[12] R.L. Johnson, C.A. Ohlin, K. Pellegrini, P.C. Burns, W.H. Casey, Dynamics of a nanometer-sized uranyl cluster in solution, Angew. Chem. Int. Ed. 52 (2013) 7464–7467.
[13] S.J. Harley, C.A. Ohlin, R.L. Johnson, A.F. Panasci, W.H. Casey, The pressure dependence of oxygen isotope exchange rates between solution and apical oxygen atoms on the $[UO_2(OH)_4]^{2-}$ ion, Angew. Chem. Int. Ed. 50 (2011) 4467–4469.
[14] R.L. Johnson, S.J. Harley, C.A. Ohlin, A.F. Panasci, W.H. Casey, Multinuclear NMR study of the pressure dependence for carbonate exchange in the $UO_2(CO_3)_3^{4-}$(aq) ion, Chemphyschem 12 (2011) 2903–2906.
[15] T.J. Swift, R.E. Connick, NMR: relaxation mechanisms of O^{17} in aqueous solutions of paramagnetic cations and the lifetime of water molecules in the first coordination sphere, J. Chem. Phys. 37 (1962) 307–320.
[16] J. Maigut, R. Meier, A. Zahl, R.v. Eldik, Triggering water exchange mechanisms via chelate architecture. Shielding of transition metal centers by aminopolycarboxylate spectator ligands, J. Am. Chem. Soc. 130 (2008) 14556–14569.
[17] J.F. Keggin, Structure of the molecule of 12-phosphotungstic acid, Nature 131 (1933) 908–909.
[18] J.F. Keggin, The structure and formula of 12-phosphotungstic acid, Proc. R. Soc. Lond. A 144 (1934) 75.
[19] M.T. Pope, Heteropoly and Isopoly Oxometalates, Springer-Verlag, Berlin, 1983.

[20] W.F. Hillebrand, H.E. Merwin, F.E. Wright, Hewettite, metahewettite, and pascoite, hydrous calcium vanadates, Z. Kristallogr. 54 (1914) 209–231.
[21] J.M. Hughes, M. Schindler, J. Rakovan, F.E. Cureton, The crystal structure of hummerite, $KMg(V_5O_{14}).8H_2O$: bonding between the $[V_{10}O_{28}]^{6-}$ structural unit and the $[K_2Mg_2(H_2O)_{16}]^{+}$ interstitial complex, Can. Mineral. 40 (2002) 1429–1435.
[22] J.M. Hughes, W.S. Wise, M.E. Gunter, J.P. Morton, J. Rakovan, Lasalite, $Na_2Mg_2[V_{10}O_{28}].20H_2O$, a new decavanadate mineral species from the Vanadium Queen mine, La Sal District, Utah: description, atomic arrangement, and relationship to the pascoite group of minerals, Can. Mineral. 46 (2008) 1365–1372.
[23] A.R. Kampf, I.M. Steele, Magnesiopascoite, a new member of the pascoite group: description and crystal structure, Can. Mineral. 46 (2008) 679–686.
[24] M.A. Cooper, Y.A. Abdu, N.A. Ball, P. Černý, F.C. Hawthorne, R. Kristiansen, Aspedamite, ideally $[\ ]_{12}(Fe^{3+},Fe^{2+})3Nb_4[Th(Nb,Fe^{3+})_{12}O_{42}]_{12}[(H_2O),(OH)]_{12}$, a new heteropolyniobate mineral species from the Herrebøkasa quarry, Aspedammen, Østfold, Southern Norway: description and crystal structure, Can. Mineral. 50 (2012) 793–804.
[25] H. Friis, M.T. Weller, A.R. Kampf, Hansesmarkite, $Ca_2Mn_2Nb_6O_{19}{\cdot}20H_2O$, a new hexaniobate from a syenite pegmatite in the Larvik plutonic complex, southern Norway, Mineral. Mag. 81 (2017) 543–554.
[26] P.C. Burns, K.-A. Kubatko, G. Sigmon, B.J. Fryer, J.E. Gagnon, M.R. Antonio, L. Soderholm, Actinyl peroxide nanospheres, Angew. Chem. Int. Ed. 44 (2005) 2135–2139.
[27] T.Z. Forbes, J.G. McAlpine, R. Murphy, P.C. Burns, Metal-oxygen isopolyhedra assembled into fullerene topologies, Angew. Chem. Int. Ed. 47 (2008) 2710–2711.
[28] J. Qiu, P.C. Burns, Clusters of actinides with oxide, peroxide, or hydroxide bridges, Chem. Rev. 113 (2013) 1097–1120.
[29] K.-A. Hughes Kubatko, K.B. Helean, A. Navrotsky, P.C. Burns, Stability of peroxide-containing uranyl minerals, Science 302 (2003) 1191–1194.
[30] C.L. Hill, L. Delannoy, D.C. Duncan, I.A. Weinstock, R.F. Renneke, R.S. Reiner, R.H. Atalla, J.W. Han, D.A. Hillesheim, R. Cao, T.M. Anderson, N.M. Okun, D.G. Musaev, Y.V. Geletii, Complex catalysts from self-repairing ensembles to highly reactive air-based oxidation systems, C. R. Chim. 10 (2007) 305–312.
[31] C.L. Hill, Progress and challenges in polyoxometalate-based catalysis and catalytic materials chemistry, J. Mol. Cat. A 262 (2007) 2–6.
[32] C.L. Hill, N.M. Okun, D.A. Hillesheim, Y.V. Geletii, Catalysts for aerobic decontamination of chemical warfare agents under ambient conditions, ACS Symposium Series, vol. 980, American Chemical Society, 2007, pp. 198–209.
[33] C.L. Hill, Stable, self-assembling, equilibrating catalysts for green chemistry, Angew. Chem. Int. Ed. 43 (2004) 402–404.
[34] C.L. Hill, J.A. McCleverty, T.J. Meyer (Eds.), Polyoxometalates: Reactivity, Comprehensive Coordination Chemistry II, vol. 4, Pergamon, 2004, pp. 679–759.
[35] I.M. Mbomekalle, B. Keita, L. Nadjo, P. Berthet, W.A. Neiwert, C.L. Hill, M.D. Ritorto, T.M. Anderson, Manganous heteropolytungstates. Synthesis and heteroatom effects in Wells-Dawson-derived sandwich complexes, Dalton Trans. (2003) 2646–2650.
[36] I.M. Mbomekalle, B. Keita, L. Nadjo, P. Berthet, K.I. Hardcastle, C.L. Hill, T.M. Anderson, Multi-iron tungstodiarsenates. Synthesis, characterization, and electrocatalytic studies of αββα-$(Fe^{III}OH_2)_2Fe^{III}_2(As_2W_{15}O_{56})^{12-}_2$, Inorg. Chem. 42 (2003) 1163–1169.
[37] X. Fang, T.M. Anderson, W.A. Neiwert, C.L. Hill, Yttrium polyoxometalates. Synthesis and characterization of a carbonate-encapsulated sandwich-type complex, Inorg. Chem. 42 (2003) 8600–8602.

[38] T.M. Anderson, C.L. Hill, Modeling reactive metal oxides. Kinetics, thermodynamics, and mechanism of M_3 cap isomerization in polyoxometalates, Inorg. Chem. 41 (2002) 4252–4258.
[39] C.L. Hill, Polyoxometalates—multicomponent molecular vehicles to probe fundamental issues and practical problems, Chem. Rev. 98 (1998) 1–2.
[40] I.A. Weinstock, R.H. Atalla, R.S. Reiner, M.A. Moen, K.E. Hammel, C.J. Houtman, C.L. Hill, M.K. Harrup, A new environmentally benign technology for transforming wood pulp into paper. Engineering polyoxometalates as catalysts for multiple processes, J. Mol. Catal. A 116 (1997) 59–84.
[41] J.T. Rhule, C.L. Hill, D.A. Judd, R.F. Schinazi, Polyoxometalates in medicine, Chem. Rev. 98 (1993) 327–358.
[42] A.D. English, J.P. Jesson, W.G. Klemperer, T. Mamouneas, L. Messerle, W. Shum, A. Tramontano, Solution structures of large group 5A and 6A polyoxoanions by oxygen-17 nuclear magnetic resonance, J. Am. Chem. Soc. 97 (1975) 4785–4786.
[43] M. Filowitz, W.G. Klemperer, Oxygen-17 nuclear magnetic resonance structure determinations of $As_2Mo_6O_{26}^{6-}$ and $(PhAs)_2Mo_6O_{24}^{4-}$, Chem. Commun. (1976) 233–234.
[44] M. Filowitz, R.K.C. Ho, W.G. Klemperer, W. Shum, Oxygen-17 nuclear magnetic resonance spectroscopy of polyoxometalates. 1. Sensitivity and resolution, Inorg. Chem. 18 (1979) 93–103.
[45] V.W. Day, W.G. Klemperer, Metal oxide chemistry in solution: the early transition metal polyoxoanions, Science 228 (1985) 533–541.
[46] K. Piepgrass, J.N. Barrows, M.T. Pope, Oxygen-17 NMR of paramagnetic heteropoly blues. Discrimination between electron delocalization pathways and between intermolecular electron transfer rates, Chem. Commun. (1989) 10–12.
[47] K.W. Piepgrass, NMR Studies and Oxygen Transfer Chemistry of Heteropoly Browns. Oxygen-17 NMR Studies of Keggin Tungstates, Georgetown University, 1989, p. 248.
[48] A.R. Thompson, A.C. Kunwar, H.S. Gutowsky, E. Oldfield, O-17 and Al-27 nuclear-magnetic-resonance spectroscopic investigations of aluminum(III) hydrolysis products, Dalton Trans. (1987) 2317–2322.
[49] O.W. Howarth, M. Jarrold, Protonation of the decavanadate(6-) ion: a vanadium-51 nuclear magnetic resonance study, Dalton Trans. (1978) 503–506.
[50] E. Heath, O.W. Howarth, Vanadium-51 and oxygen-17 nuclear magnetic resonance study of vanadate(V) equilibria and kinetics, Dalton Trans. (1981) 1105–1110.
[51] L. Pettersson, B. Hedman, I. Andersson, N. Ingri, Multicomponent polyanions. 34. A potentiometric and vanadium-51 NMR study of equilibria in the H^+-HVO_4^{2-} system in 0.6 M sodium chloride medium covering the range $1 < -\lg[H+] < 10$, Chem. Scr. 22 (1983) 254–264.
[52] A.T. Harrison, O.W. Howarth, Oxygen exchange and protonation of polyanions: a multinuclear magnetic resonance study of tetradecavanadophosphate(9-) and decavanadate(6-), Dalton Trans. (1985) 1953–1957.
[53] A.T. Harrison, O.W. Howarth, High-field vanadium-51 and oxygen-17 NMR study of peroxovanadates(V), Dalton Trans. 1985 (1985) 1173–1177.
[54] O.W. Howarth, L. Pettersson, I. Andersson, Aqueous molybdovanadates at high molybdenum: vanadium ratio, Dalton Trans. (1991) 1799–1812.
[55] O.W. Howarth, New aspects of NMR spectroscopy of polyoxometalates, Mol. Eng. 3 (1993) 131–140.
[56] I. Andersson, J.J. Hastings, O.W. Howarth, L. Pettersson, Aqueous tungstovanadate equilibria, Dalton Trans. (1996) 2705–2711.
[57] I.A. Weinstock, J.J. Cowan, E.M.G. Barbuzzi, H. Zeng, C.L. Hill, Equilibria between α and β isomers of Keggin Heteropolytungstates, J. Am. Chem. Soc. 121 (1993) 4608–4617.

[58] J.J. Cowan, A.J. Bailey, R.A. Heintz, B.T. Do, K.I. Hardcastle, C.L. Hill, I.A. Weinstock, Formation, isomerization, and derivatization of Keggin tungstoaluminates, Inorg. Chem. 40 (2001) 6666–6675.
[59] A. Czap, N.I. Neuman, T.W. Swaddle, Electrochemistry and homogeneous self-exchange kinetics of the aqueous 12-tungstoaluminate(5-/6-) couple, Inorg. Chem. 45 (2006) 9518–9530.
[60] W.H. Casey, Large aqueous aluminum hydroxide molecules, Chem. Rev. 106 (2006) 1–16.
[61] C.A. Ohlin, S.J. Harley, J.G. McAlpin, R.K. Hocking, B.Q. Mercado, R.L. Johnson, E.M. Villa, M.K. Fidler, M.M. Olmstead, L. Spiccia, R.D. Britt, W.H. Casey, Rates of water exchange for two cobalt(II) heteropolyoxotungstate compounds in aqueous solution, Chem. A Eur. J. 17 (2011) 4408–4417.
[62] R. Sharma, J. Zhang, C. Andre Ohlin, pH-dependent solution dynamics of a manganese(ii) polyoxometalate, $[Mn_4(H_2O)_2(P_2W_{15}O_{56})_2]^{16-}$, and $[Mn(H_2O)_6]^{2+}$, Dalton Trans. 44 (2015) 19068–19071.
[63] D. Lieb, A. Zahl, E.F. Wilson, C. Streb, L.C. Nye, K. Meyer, I. Ivanović-Burmazović, Water exchange reactivity and stability of cobalt polyoxometalates under catalytically relevant pH conditions: insight into water oxidation catalysis, Inorg. Chem. 50 (2011) 9053–9058.
[64] D. Hugi-Cleary, L. Helm, A.E. Merbach, High-pressure NMR kinetics 24. Variable-temperature and variable-pressure ^{17}O-NMR study of water exchange of hexaaquaaluminum(III), Helv. Chim. Acta 68 (1985) 545–554.
[65] D.T. Richens, The Chemistry of Aqua Ions, John Wiley, New York, 1997, pp. 592.
[66] R.K. Murmann, Rate of oxygen exchange between the perrhenate ion and water, J. Phys. Chem. 71 (1967) 974–978.
[67] R.K. Murmann, Oxygen-18 exchange studies on vanadate ($V_{10}O_{28}^{6-}$) in aqueous media, J. Am. Chem. Soc. 96 (1974) 7836.
[68] R.K. Murmann, K.C. Giese, Mechanism of oxygen-18 exchange between water and the vanadium(V) oxyanion: $V_{10}O_{28}^{6-}$, Inorg. Chem. 17 (1978) 1160–1166.
[69] P. Comba, L. Helm, The solution structure and reactivity of decavanadate, Helv. Chim. Acta 71 (1988) 1406–1420.
[70] W.G. Klemperer, K.A. Marek, An ^{17}O NMR study of hydrolyzed Nb^{V} in weakly acidic and basic aqueous solutions, Eur. J. Inorg. Chem. 2013 (2013) 1762–1771.
[71] E.M. Villa, C.A. Ohlin, E. Balogh, T.M. Anderson, M.D. Nyman, W.H. Casey, Adding reactivity to structure-reaction dynamics in a nanometer-size oxide ion in water, Am. J. Sci. 308 (2008) 942–953.
[72] E.M. Villa, C.A. Ohlin, W.H. Casey, Oxygen-isotope exchange rates for three iso-structural polyoxometalate ions, J. Am. Chem. Soc. 132 (2010) 5264–5272.
[73] J.R. Rustad, W.H. Casey, Metastable structures and isotope exchange reactions in polyoxometalate ions provide a molecular view of oxide dissolution, Nat. Mater. 11 (2012) 223–226.
[74] W.H. Casey, J.R. Rustad, Pathways for oxygen-isotope exchange in two model oxide clusters, New J. Chem. 40 (2016) 898–905.
[75] Q. Yin, J.M. Tan, C. Besson, Y.V. Geletii, D.G. Musaev, A.E. Kuznetsov, Z. Luo, K.I. Hardcastle, C.L. Hill, A fast soluble carbon-free molecular water oxidation catalyst based on abundant metals, Science 328 (2010) 342.
[76] S.S. Acharya, B. Winther-Jensen, L. Spiccia, C.A. Ohlin, Rates of water exchange in 2,2'-bipyridine and 1,10-phenanthroline complexes of Co^{II} and Mn^{II}, Aust. J. Chem. 70 (2017) 751–754.
[77] A.F. Panasci, C.A. Ohlin, S.J. Harley, W.H. Casey, Rates of water exchange on the $[Fe_4(OH)_2(hpdta)_2(H_2O)_4]^0$ molecule and its implications for geochemistry, Inorg. Chem. 51 (2012) 6731–6738.

[78] M. Botta, S. Avedano, G.B. Giovenzana, A. Lombardi, D. Longo, C. Cassino, L. Tei, S. Aime, Relaxometric study of a series of monoaqua Gd^{III} complexes of rigidified EGTA-like chelators and their noncovalent interaction with human serum albumin, Eur. J. Inorg. Chem. (2011) 802–810.
[79] K.H. Chalmers, M. Botta, D. Parker, Strategies to enhance signal intensity with paramagnetic fluorine-labeled lanthanide complexes as probes for ^{19}F magnetic resonance, Dalton Trans. 40 (2011) 904–913.
[80] Y.-H. Chang, C.-Y. Chen, G. Singh, H.-Y. Chen, G.-C. Liu, Y.-G. Goan, S. Aime, Y.-M. Wang, Synthesis and physicochemical characterization of carbon backbone modified $[Gd(TTDA)(H_2O)]^{2-}$ derivatives, Inorg. Chem. 50 (2011) 1275–1287.
[81] L. Tei, G. Gugliotta, M. Fekete, F.K. Kalman, M. Botta, Mn(II) complexes of novel hexadentate AAZTA-like chelators: a solution thermodynamics and relaxometric study, Dalton Trans. 40 (2011) 2025–2032.
[82] C. Vanasschen, N. Bouslimani, D. Thonon, J.F. Desreux, Gadolinium DOTA chelates featuring alkyne groups directly grafted on the tetraaza macrocyclic ring: synthesis, relaxation properties, "click" reaction, and high-relaxivity micelles, Inorg. Chem. 50 (2011) 8946–8958.
[83] Z. Baranyai, L. Tei, G.B. Giovenzana, F.K. Kalman, M. Botta, Equilibrium and NMR relaxometric studies on the s-Triazine-based heptadentate ligand PTDITA showing high selectivity for Gd^{3+} ions, Inorg. Chem. 51 (2012) 2597–2607.
[84] T. Chauvin, S. Torres, R. Rosseto, J. Kotek, B. Badet, P. Durand, E. Toth, Lanthanide(III) complexes that contain a self-immolative arm: potential enzyme responsive contrast agents for magnetic resonance imaging, Chem. A Eur. J. 18 (2012) 1408–1418.
[85] D. Esteban-Gomez, A. de Blas, T. Rodriguez-Blas, L. Helm, C. Platas-Iglesias, Hyperfine coupling constants on inner-sphere water molecules of Gd^{III}-based MRI contrast agents, Chemphyschem 13 (2012) 3640–3650.
[86] A. Forgacs, G.B. Giovenzana, M. Botta, E. Bruecher, I. Toth, Z. Baranyai, Influence of gem-dimethyl substitution on the stability, kinetics and relaxometric properties of PDTA complexes, Eur. J. Inorg. Chem. 2012 (2012) 2074–2086.
[87] F. Mayer, C. Platas-Iglesias, L. Helm, J.A. Peters, K. Djanashvili, ^{17}O NMR and density functional theory study of the dynamics of the carboxylate groups in DOTA complexes of lanthanides in aqueous solution, Inorg. Chem. 51 (2012) 170–178.
[88] F.A. Rojas-Quijano, G. Tircso, E. Tircsone Benyo, Z. Baranyai, H. Tran Hoang, F.K. Kalman, P.K. Gulaka, V.D. Kodibagkar, S. Aime, Z. Kovacs, A.D. Sherry, Synthesis and characterization of a hypoxia-sensitive MRI probe, Chem. A Eur. J. 18 (2012) 9669–9676.
[89] L. Tei, Z. Baranyai, C. Cassino, M. Fekete, F.K. Kalman, M. Botta, Solution properties of the Ln^{III} complexes of a novel octadentate chelator with rigidified iminodiacetate arms, Dalton Trans. 41 (2012) 12797–12806.
[90] D. Lieb, F.C. Friedel, M. Yawer, A. Zahl, M.M. Khusniyarov, F.W. Heinemann, I. Ivanovic-Burmazovic, Dinuclear seven-coordinate Mn(II) complexes: effect of manganese(II)-hydroxo species on water exchange and superoxide dismutase activity, Inorg. Chem. 52 (2013) 222–236.
[91] V. Patinec, G.A. Rolla, M. Botta, R. Tripier, D. Esteban-Gomez, C. Platas-Iglesias, Hyperfine coupling constants on inner-sphere water molecules of a triazacyclononane-based Mn(II) complex and related systems relevant as MRI contrast agents, Inorg. Chem. 52 (2013) 11173–11184.
[92] M.P. Placidi, M. Botta, F.K. Kalman, G.E. Hagberg, Z. Baranyai, A. Krenzer, A.K. Rogerson, I. Toth, N.K. Logothetis, G. Angelovski, Aryl-phosphonate lanthanide complexes and their fluorinated derivatives: investigation of their unusual

relaxometric behavior and potential application as dual frequency ^{1}H/^{19}F MRI probes, Chem. A Eur. J. 19 (2013) 11644–11660.
[93] G.A. Rolla, C. Platas-Iglesias, M. Botta, L. Tei, L. Helm, ^{1}H and ^{17}O NMR relaxometric and computational study on macrocyclic Mn(II) complexes, Inorg. Chem. 52 (2013) 3268–3279.
[94] Z. Baranyai, G.A. Rolla, R. Negri, A. Forgacs, G.B. Giovenzana, L. Tei, Comprehensive evaluation of the physicochemical properties of Ln^{III} complexes of aminoethyl-DO3A as pH-responsive T1-MRI contrast agents, Chem. A Eur. J. 20 (2014) 2933–2944.
[95] B. Chahid, L. Vander Elst, J. Flament, F. Boumezbeur, C. Medina, M. Port, R.N. Muller, S. Lesieur, Entrapment of a neutral Tm(III)-based complex with two inner-sphere coordinated water molecules into PEG-stabilized vesicles: towards an alternative strategy to develop high-performance LipoCEST contrast agents for MR imaging, Contrast Media Mol. Imaging 9 (2014) 391–399.
[96] D. Esteban-Gomez, C. Cassino, M. Botta, C. Platas-Iglesias, ^{17}O and ^{1}H relaxometric and DFT study of hyperfine coupling constants in $[Mn(H_2O)_6]^{2+}$, RSC Adv. 4 (2014) 7094–7103.
[97] L. Fusaro, M. Luhmer, An oxygen-17 dynamic NMR study of the Pr-DOTA complex, Dalton Trans. 43 (2014) 967–972.
[98] R. Negri, Z. Baranyai, L. Tei, G.B. Giovenzana, C. Platas-Iglesias, A.C. Benyei, J. Bodnar, A. Vagner, M. Botta, Lower denticity leading to higher stability: structural and solution studies of Ln(III)-OBETA somplexes, Inorg. Chem. 53 (2014) 12499–12511.
[99] M. Elhabiri, S. Abada, M. Sy, A. Nonat, P. Choquet, D. Esteban-Gomez, C. Cassino, C. Platas-Iglesias, M. Botta, L.J. Charbonniere, Importance of outer-sphere and aggregation phenomena in the relaxation properties of phosphonated gadolinium complexes with potential applications as MRI contrast agents, Chem. A Eur. J. 21 (2015) 6535–6546.
[100] R.V. Southwood-Jones, W.L. Earl, K.E. Newman, A.E. Merbach, Oxygen-17 NMR and EPR studies of water exchange from the first coordination sphere of gadolinium(III) aquoion and gadolinium(III) propylenediaminetetraacetate, J. Chem. Phys. 73 (2015) 5909–5918.
[101] W. Zhang, J.A. Peters, F. Mayer, L. Helm, K. Djanashvili, Prototropic exchange governs T_1 and T_2 relaxivities of a potential MRI contrast agent nanozeolite Gd-LTL with a high pH responsiveness, J. Phys. Chem. C 119 (2015) 5080–5089.
[102] A. Forgacs, L. Tei, Z. Baranyai, I. Toth, L. Zekany, M. Botta, A bisamide derivative of [Mn(1,4-DO2A)]—solution thermodynamic, kinetic, and NMR relaxometric studies, Eur. J. Inorg. Chem. 2016 (2016) 1165–1174.
[103] V.R. Mundlapati, P. Jena, A.N. Acharya, A.K. Kar, A.C. Dash, H.S. Biswal, Water exchange reaction of a manganese catalase mimic: oxygen-17 NMR relaxometry study on (aqua)manganese(III) in a salen scaffold and its reactions in a mildly basic medium, RSC Adv. 6 (2016) 111739–111746.
[104] J.A. Peters, The reliability of parameters obtained by fitting of ^{1}H NMRD profiles and ^{17}O NMR data of potential Gd^{3+}-based MRI contrast agents, Contrast Media Mol. Imaging 11 (2016) 160–168.
[105] A. Forgacs, L. Tei, Z. Baranyai, D. Esteban-Gomez, C. Platas-Iglesias, M. Botta, Optimising the relaxivities of Mn^{2+} complexes by targeting human serum albumin (HSA), Dalton Trans. 46 (2017) 8494–8504.
[106] E. Molnar, B. Varadi, Z. Garda, R. Botar, F.K. Kalman, E. Toth, C. Platas-Iglesias, I. Toth, E. Brucher, G. Tircso, Remarkable differences and similarities between the isomeric Mn(II)-cis- and trans-1,2-diaminocyclohexane-N,N,N',N'-tetraacetate

complexes. Inorg. Chim. Acta 472 (2017) 254–263, https://doi.org/10.1016/j.ica.2017.07.071.
[107] C. Vanasschen, E. Molnar, G. Tircso, F.K. Kalman, E. Toth, M. Brandt, H.H. Coenen, B. Neumaier, Novel CDTA-based, bifunctional chelators for stable and inert Mn^{II} complexation: synthesis and physicochemical characterization, Inorg. Chem. 56 (2017) 7746–7760.
[108] A. Wacker, F. Carniato, C. Platas-Iglesias, D. Esteban-Gomez, H.-J. Wester, L. Tei, J. Notni, Dimer formation of GdDO3A-arylsulfonamide complexes causes loss of pH-dependency of relaxivity, Dalton Trans. 46 (2017) 16828–16836.
[109] R.L. Johnson, E.M. Villa, C.A. Ohlin, J.R. Rustad, W.H. Casey, ^{17}O NMR and computational study of a tetrasiliconiobate ion, $[H_{2+x}Si_4Nb_{16}O_{56}]^{(14-x)-}$, Chem. A Eur. J. 17 (2011) 9359–9367.
[110] E.M. Villa, C.A. Ohlin, J.R. Rustad, W.H. Casey, Isotope-exchange dynamics in isostructural decametalates with profound differences in reactivity, J. Am. Chem. Soc. 131 (2009) 16488–16492.
[111] E.M. Villa, C.A. Ohlin, W.H. Casey, Borate accelerates rates of steady oxygen-isotope exchange for polyoxoniobate ions in water, Chem. A Eur. J. 16 (2010) 8631–8634.
[112] J.R. Black, M. Nyman, W.H. Casey, Rates of oxygen exchange between the $[H_xNb_6O_{19}]^{8-x}(aq)$ Lindqvist ion and aqueous solutions, J. Am. Chem. Soc. 128 (2006) 14712–14720.
[113] C.A. Ohlin, E.M. Villa, J.C. Fettinger, W.H. Casey, Distinctly different reactivities of two similar polyoxoniobates with hydrogen peroxide, Angew. Chem. Int. Ed. 47 (2008) 8251–8254.
[114] R.I. Maksimovskaya, G.M. Maksimov, Borotungstate polyoxometalates: multinuclear NMR structural characterization and conversions in solutions, Inorg. Chem. 50 (2011) 4725–4731.
[115] B. Kandasamy, C. Wills, W. McFarlane, W. Clegg, R.W. Harrington, A. Rodríguez-Fortea, J.M. Poblet, P.G. Bruce, R.J. Errington, An alkoxido-tin-substituted polyoxometalate $[(MeO)SnW_5O_{18}]^{3-}$: the first member of a new family of reactive $\{SnW_5\}$ Lindqvist-type anions, Chem. A Eur. J. 18 (2012) 59–62.
[116] L. Coyle, P.S. Middleton, C.J. Murphy, W. Clegg, R.W. Harrington, R.J. Errington, Protonolysis of $[(iPrO)TiMo_5O_{18}]^{3-}$: access to a family of $TiMo_5$ Lindqvist type polyoxometalates, Dalton Trans. 41 (2012) 971–981.
[117] K.P. O'Halloran, C. Zhao, N.S. Ando, A.J. Schultz, T.F. Koetzle, P.M.B. Piccoli, B. Hedman, K.O. Hodgson, E. Bobyr, M.L. Kirk, S. Knottenbelt, E.C. Depperman, B. Stein, T.M. Anderson, R. Cao, Y.V. Geletii, K.I. Hardcastle, D.G. Musaev, W.A. Neiwert, X. Fang, K. Morokuma, S. Wu, P. Kögerler, C.L. Hill, Revisiting the polyoxometalate-based late-transition-metal-oxo complexes: the "Oxo Wall" stands, Inorg. Chem. 51 (2012) 7025–7031.
[118] A. Drljaca, A. Zahl, R. Van Eldik, High-pressure oxygen-17 NMR study of the dihydroxo-bridged rhodium(III) hydrolytic dimer. Mechanistic evidence for limiting dissociative water exchange pathways, Inorg. Chem. 37 (1998) 3948–3953.
[119] A. Cusanelli, U. Frey, D.T. Richens, A.E. Merbach, The slowest water exchange at a homoleptic mononuclear metal center: variable-temperature and variable-pressure 17O NMR study on $[Ir(H_2O)_6]^{3+}$, J. Am. Chem. Soc. 118 (1996) 5265–5271.
[120] J. Burgess, Metal Ions in Solution, Ellis Horwood Limited, Chiehester, England, 1978464 pp.
[121] J. Burgess, Ions in Solution: Basic Principles of Chemical Interactions, Ellis-Horwood Limited, Chichester, 1988.
[122] R.G. Wilkins, The Study of Kinetics and Mechanism of Reactions of Transition Metal Complexes, VCH, 1991, p. 465.

[123] R. Van Eldik, T. Asano, W.J. Le Noble, Activation and reaction volumes in solution. 2, Chem. Rev. 89 (1989) 549–688.
[124] A. Drljaca, C.D. Hubbard, R. Van Eldik, T. Asano, M.V. Basilevsky, W.J. Le Noble, Activation and reaction volumes in solution. 3, Chem. Rev. 98 (1998) 2167–2289.
[125] E.L. Shock, D.C. Sassani, M. Willis, D.A. Sverjensky, Inorganic species in geologic fluids: correlations among standard molal thermodynamic properties of aqueous ions and hydroxide complexes, Geochim. Cosmochim. Acta 61 (1997) 907–950.
[126] D.A. Sverjensky, E.L. Shock, H.C. Helgeson, Prediction of the thermodynamic properties of aqueous metal complexes to 1000°C and 5 kb, Geochim. Cosmochim. Acta 61 (1997) 1359–1412.
[127] A.V. Plyasunov, J.P. O'Connell, R.H. Wood, E.L. Shock, Infinite dilution partial molar properties of aqueous solutions of nonelectrolytes. II. Equations for the standard thermodynamic functions of hydration of volatile nonelectrolytes over wide ranges of conditions including subcritical temperatures, Geochim. Cosmochim. Acta 64 (2000) 2779–2795.
[128] M.D. Schulte, E.L. Shock, R.H. Wood, The temperature dependence of the standard-state thermodynamic properties of aqueous nonelectrolytes, Geochim. Cosmochim. Acta 65 (2001) 3919–3930.
[129] P.A. Canovas, E.L. Shock, Geobiochemistry of metabolism: standard state thermodynamic properties of the citric acid cycle, Geochim. Cosmochim. Acta 195 (2016) 293–322.
[130] D. Pan, L. Spanu, B. Harrison, D.A. Sverjensky, G. Galli, Dielectric properties of water under extreme conditions and transport of carbonates in the deep earth, Proc. Natl. Acad. Sci. U.S.A. 110 (2013) 6646–6650.
[131] D.A. Sverjensky, B. Harrison, D. Azzolini, Water in the deep earth: the dielectric constant and the solubilities of quartz and corundum to 60 kb and 1200°C, Geochim. Cosmochim. Acta 129 (2014) 125–145.
[132] D.A. Sverjensky, F. Huang, Diamond formation due to a pH drop during fluid-rock interactions, Nat. Commun. 6 (2015) 8702.
[133] H. C. Helgeson, D. H. Kirkham and G. C. Flowers, Theoretical prediction of the thermodynamic behavior of aqueous electrolytes at high pressures and temperatures, Parts I-IV, Am. J. Sci. Special Volume of Reprinted Articles: 274, 1089–1198; 274, 1199–1261; 276, 97–240; 281, 1249–1516. (1994).
[134] M. Filowitz, W.G. Klemperer, L. Messerle, W. Shum, An oxygen-17 nuclear magnetic resonance chemical shift scale for polyoxomolybdates, J. Am. Chem. Soc. 98 (1976) 2345–2346.
[135] B.G. Pautler, C.A. Colla, R.L. Johnson, P. Klavins, S.J. Harley, C.A. Ohlin, D.A. Sverjensky, J.H. Walton, W.H. Casey, A high-pressure NMR probe for aqueous geochemistry, Angew. Chem. Int. Ed. 53 (2014) 9962.
[136] G. Ochoa, C.D. Pilgrim, M.N. Martin, C.A. Colla, P. Klavins, M.P. Augustine, W.H. Casey, ^{2}H and ^{139}La NMR spectroscopy in aqueous solutions at geochemical pressures, Angew. Chem. Int. Ed. 54 (2015) 15444–15447.
[137] G. Ochoa, C.A. Colla, P. Klavins, M.P. Augustine, W.H. Casey, NMR spectroscopy of some electrolyte solutions to 1.9 GPa, Geochim. Cosmochim. Acta 193 (2016) 66–74.
[138] M.P. Augustine, G. Ochoa, W.H. Casey, Steps to achieving high-resolution NMR spectroscopy on solutions at GPa pressure, Am. J. Sci. 317 (2017) 846–860.
[139] N. Aslam, M. Pfender, P. Neumann, R. Reuter, A. Zappe, F. Fávaro de Oliveira, A. Denisenko, H. Sumiya, S. Onoda, J. Isoya, J. Wrachtrup, Nanoscale nuclear magnetic resonance with chemical resolution, Science 357 (2017) 67–71.

[140] E.H. Abramson, Viscosity of water measured to pressures of 6 GPa and temperatures of 300°C, Phys. Rev. E 76 (2007), 051203.
[141] Y. Lee, J. Jonas, Effect of pressure on proton spin-lattice relaxation in several concentrated aqueous electrolyte solutions, J. Magn. Reson. 5 (1971) 267–272.
[142] J. Jonas, T. DeFries, D.J. Wilbur, Molecular motions in compressed liquid water, J. Chem. Phys. 65 (1976) 582–588.
[143] T. DeFries, J. Jonas, Molecular motions in compressed liquid heavy water at low temperatures, J. Chem. Phys. 66 (1977) 5393–5399.
[144] J.A. Akai, J. Jonas, The effect of pressure and temperature on self-diffusion coefficients in several concentrated deuterium oxide diamagnetic electrolyte solutions, J. Solution Chem. 5 (1978) 563–574.
[145] J. Jonas, Nuclear magnetic resonance studies at high pressures, Rev. Phys. Chem. Jpn. 50 (1980) 19–35.
[146] W.J. Lamb, G.A. Hoffman, J. Jonas, Self-diffusion in compressed supercritical water, J. Chem. Phys. 74 (1981) 6875–6880.
[147] M. Matsumoto, T.W. Swaddle, The decamethylferrocene(+/0) electrode reaction in organic solvents at variable pressure and temperature, Inorg. Chem. 43 (2004) 2724–2735.
[148] L. Ballard, C. Reiner, J. Jonas, High-resolution NMR probe for experiments at high pressures, J. Magn. Reson. 123 (1996) 81–86.
[149] W.G. Klemperer, W. Shum, Isomerism and charge distribution in mixed-metal polyoxoanion clusters: oxygen-17 nuclear magnetic resonance structure determinations of cis-$V_2W_4O_{19}^{4-}$ and cis-$HV_2W_4O_{19}^{3-}$, J. Am. Chem. Soc. 100 (1978) 4891–4893.
[150] L. Ballard, A. Yu, C. Reiner, J. Jonas, A high-pressure, high-resolution NMR probe for experiments at 500 MHz, J. Magn. Reson. 133 (1998) 190–193.
[151] H. Fukui, Theory and calculation of nuclear shielding constants, Prog. Nucl. Magn. Reson. Spectrosc. 31 (1997) 317–342.
[152] G. Schreckenbach, T. Ziegler, Calculation of NMR shielding tensors using gauge-including atomic orbitals and modern density functional theory, J. Phys. Chem. 99 (1995) 606–611.
[153] H. Fukui, K. Miura, H. Shinbori, Calculation of NMR chemical shifts. VI. Gauge invariant and Hermitian condition, J. Chem. Phys. 83 (1985) 907–908.
[154] F. London, Théorie quantique des courants interatomiques dans les combinaisons aromatiques, J. Phys. Radium 8 (1937) 397–409.
[155] P.J. Wilson, R.D. Amos, N.C. Handy, Toward coupled-cluster accuracy in the prediction of nuclear shielding constants: a simple and efficient DFT approach, Chem. Phys. Lett. 312 (1999) 475–484.
[156] R. van Meer, O.V. Gritsenko, E.J. Baerends, Physical meaning of virtual Kohn–Sham orbitals and orbital energies: an ideal basis for the description of molecular excitations, J. Chem. Theory Comput. 10 (2014) 4432–4441.
[157] P.R.T. Schipper, O.V. Gritsenko, S.J.A. van Gisbergen, E.J. Baerends, Molecular calculations of excitation energies and (hyper)polarizabilities with a statistical average of orbital model exchange-correlation potentials, J. Chem. Phys. 112 (2000) 1344–1352.
[158] N. Vankova, T. Heine, U. Kortz, NMR chemical shifts of metal centres in polyoxometalates: relativistic DFT predictions, Eur. J. Inorg. Chem. 2009 (2009) 5102–5108.
[159] N.V. Izarova, N. Vankova, A. Banerjee, G.B. Jameson, T. Heine, F. Schinle, O. Hampe, U. Kortz, A noble-metalate bowl: the polyoxo-6-vanado(V)-7-palladate(II) $[Pd_7V_6O_{24}(OH)_2]^{6-}$, Angew. Chem. Int. Ed. 49 (2010) 7807–7811.
[160] M. Swart, M. Solà, F.M. Bickelhaupt, A new all-round density functional based on spin states and S_N2 barriers, J. Chem. Phys. 131 (2009), 094103.

[161] C. van Wullen, A comparison of density functional methods for the calculation of phosphorus-31 NMR chemical shifts, Phys. Chem. Chem. Phys. 2 (2000) 2137–2144.
[162] M. Pascual-Borràs, X. Lopez, J.M. Poblet, Accurate calculation of ^{31}P NMR chemical shifts in polyoxometalates, Phys. Chem. Chem. Phys. 17 (2015) 8723–8731.
[163] G. te Velde, F.M. Bickelhaupt, E.J. Baerends, C. Fonseca Guerra, S.J.A. van Gisbergen, J.G. Snijders, T. Ziegler, Chemistry with ADF, J. Comput. Chem. 22 (2001) 931–967.
[164] M.R. Antonio, M. Nyman, T.M. Anderson, Direct observation of contact ion-pair formation in aqueous solution, Angew. Chem. Int. Ed. 48 (2009) 6136–6140.
[165] J. Gracia, J.M. Poblet, J. Autschbach, L.P. Kazansky, Density-functional calculation of the ^{183}W and ^{17}O NMR chemical shifts for large polyoxotungstates, Eur. J. Inorg. Chem. 2006 (2006) 1139–1148.
[166] J. Gracia, J.M. Poblet, J.A. Fernández, J. Autschbach, L.P. Kazansky, DFT calculations of the ^{183}W NMR chemical shifts in reduced polyoxotungstates, Eur. J. Inorg. Chem. 2006 (2006) 1149–1154.
[167] L. Vilà-Nadal, J.P. Sarasa, A. Rodríguez-Fortea, J. Igual, L.P. Kazansky, J.M. Poblet, Towards the accurate calculation of ^{183}W NMR chemical shifts in polyoxometalates: the relevance of the structure, Chem. Asian J. 5 (2010) 97–104.
[168] P.J. Wilson, R.D. Amos, N.C. Handy, Accurate predictions for molecular magnetizabilities and rotational g tensors using a simple and efficient DFT approach, J. Mol. Struct. 506 (2000) 335–342.
[169] T. Helgaker, P.J. Wilson, R.D. Amos, N.C. Handy, Nuclear shielding constants by density functional theory with gauge including atomic orbitals, J. Chem. Phys. 113 (2000) 2983–2989.
[170] J. Gauss, J.F. Stanton, Perturbative treatment of triple excitations in coupled-cluster calculations of nuclear magnetic shielding constants, J. Chem. Phys. 104 (1996) 2574–2583.
[171] J. Baker, K. Wolinski, M. Malagoli, D. Kinghorn, P. Wolinski, G. Magyarfalvi, S. Saebo, T. Janowski, P. Pulay, Quantum chemistry in parallel with PQS, J. Comput. Chem. 30 (2009) 317–335.
[172] J.F. Stanton, J. Gauss, J.D. Watts, W.J. Lauderdale, R.J. Bartlett, The ACES II program system, Int. J. Quantum Chem. 44 (1992) 879–894.
[173] M. Kaupp, O.L. Malkina, V.G. Malkin, The calculation of ^{17}O chemical shielding in transition metal oxo complexes. I. Comparison of DFT and ab initio approaches, and mechanisms of relativity-induced shielding, J. Chem. Phys. 106 (1997) 9201–9212.
[174] G. Schreckenbach, T. Ziegler, Calculation of NMR shielding tensors based on density functional theory and a scalar relativistic Pauli-type Hamiltonian. The application to transition metal complexes, Int. J. Quantum Chem. 61 (1997) 899–918.
[175] M. Pascual-Borràs, X. Lopez, A. Rodriguez-Fortea, R.J. Errington, J.M. Poblet, ^{17}O NMR chemical shifts in oxometalates: from the simplest monometallic species to mixed-metal polyoxometalates, Chem. Sci. 5 (2014) 2031–2042.
[176] V.W. Day, W.G. Klemperer, D.J. Maltbie, Where are the protons in $H_3V_{10}O_{28}^{3-}$? J. Am. Chem. Soc. 109 (1987) 2991–3002.
[177] R. Sharma, J. Zhang, C.A. Ohlin, Predicting ^{17}O NMR chemical shifts of polyoxometalates using density functional theory, Phys. Chem. Chem. Phys. 18 (2016) 8235–8241.
[178] Gaussian 09, Revision E.01, M.J. Frisch, G.W. Trucks, H.B. Schlegel, G.E. Scuseria, M. A. Robb, J.R. Cheeseman, G. Scalmani, V. Barone, B. Mennucci, G.A. Petersson, H. Nakatsuji, M. Caricato, X. Li, H.P. Hratchian, A.F. Izmaylov, J. Bloino, G. Zheng, J.L. Sonnenberg, M. Hada, M. Ehara, K. Toyota, R. Fukuda, J. Hasegawa, M. Ishida, T. Nakajima, Y. Honda, O. Kitao, H. Nakai, T. Vreven,

J.A. Montgomery, Jr., J.E. Peralta, F. Ogliaro, M. Bearpark, J.J. Heyd, E. Brothers, K.N. Kudin, V.N. Staroverov, R. Kobayashi, J. Normand, K. Raghavachari, A. Rendell, J.C. Burant, S. S. Iyengar, J. Tomasi, M. Cossi, N. Rega, J.M. Millam, M. Klene, J.E. Knox, J.B. Cross, V. Bakken, C. Adamo, J. Jaramillo, R. Gomperts, R.E. Stratmann, O. Yazyev, A.J. Austin, R. Cammi, C. Pomelli, J.W. Ochterski, R.L. Martin, K. Morokuma, V.G. Zakrzewski, G.A. Voth, P. Salvador, J.J. Dannenberg, S. Dapprich, A.D. Daniels, Ö. Farkas, J.B. Foresman, J.V. Ortiz, J. Cioslowski, and D.J. Fox, Gaussian, Inc., Wallingford, CT, 2009.

[179] C.A. Ohlin, E.M. Villa, J.R. Rustad, W.H. Casey, Dissolution of insulating oxide materials at the molecular scale, Nat. Mater. 9 (2010) 11–19.